Univerzita Karlova

Přírodovědecká fakulta

Fyzikální chemie

Ing. Monika Holubová

Ovlivnění tvorby amyloidních fibril nanočásticemi a polymery

Disertační práce

Školitel: RNDr. Petr Štěpánek, DrSc.

Konzultant: Mgr. Martin Hrubý, DSc.

Ústav makromolekulární chemie, AV ČR, v.v.i

Praha, 2020

Charles University

Faculty of Science

Physical chemistry

Ing. Monika Holubová

Influence of nanoparticles and polymers on the amyloid fibril formation

Doctoral thesis

Supervisor: RNDr. Petr Štěpánek, DrSc.

Advisor: Mgr. Martin Hrubý, DSc.

Institute of Macromolecular chemistry AS CR

Praha, 2020

Declaration

I declare that I have prepared the doctoral thesis independently and that I have listed all used information sources and literature. Neither this work nor a substantial part of it has been submitted for another or the same academic degree.

Prague, 26. 10. 2020

Prohlášení

Prohlašuji, že jsem doktorskou dizertační práci zpracovala samostatně a že jsem uvedla všechny použité informační zdroje a literaturu. Tato práce ani její podstatná část nebyla předložena k získání jiného nebo stejného akademického titulu.

V Praze, 26. 10. 2020

Ing. Monika Holubová

Acknowledgment

I would like to thank my supervisor RNDr. Petr Štěpánek, DrSc very much for his constant support and help throughout my PhD study. I really appreciate that I was able to become his student and learn new and new things under his guidance. His advice has always been very valuable for me and thanks to it, the work could get closer to the goal. I would also like to thank my advisor Mgr. Martin Hrubý, DSc., who always came up with a new idea at a time when I did not know what to do. I am very glad I met him and could learn from him. Thanks to both my supervisor and my advisor, I learned to work independently and not be afraid to try new things.

My colleagues from the department of Supramolecular Polymer Systems also deserve my thanks for the enthusiasm with which they approach their work and always encouraging me at work. Many thanks mainly to Mariia Rabyk and Lenka Loukotová, who prepared some of the materials for testing. Huge thanks to Volodymyr Lobaz, who measured and evaluated the data from the ITC.

I must not forget my family and friends who have always supported and encouraged me: my mother Lenka Řebíčková, who was a great role model for me because she always approaches her work with great dedication and enthusiasm, my father Jiří Řebíček, who has always been the person who listened to me, and of course, my husband Petr Holub, who supported me throughout my studies and without whom I could never go to study PhD. Thanks to him, I was able to return to work after the birth of our son Teodor and complete my PhD study.

Table of contents:

List of abbreviations

0D	zero-dimensional
1D	one-dimensional
2D	two-dimensional
AD	Alzheimer's disease
AFFFF	asymmetric flow field-flow fractionation
AFM	atomic force microscopy
ANS	autonomic nervous system
APOE	apolipoprotein E
APP	amyloid precursor protein
$A\beta_{1\text{-}42}$	amyloid beta (1-42)
B	benzoyl groups
C_{60}	fullerenes
CDs	carbon quantum dots
CIN	cinnamoyl groups
CJD	Creutzfeldt-Jakob disease
CNPs	Carbon nanospecies
CVD	chemical vapor deposition
DLS	dynamic light scattering
EA	elemental analysis
FTIR	Fourier transform infrared spectroscopy
GAGs	glycosaminoglycans
GG	glycogen
HEWL	hen egg white lysozyme
ITC	Isothermal titration calorimetry
MAN	mannan
MD	molecular dynamics
M_w	molecular weight
MWNT	multiwalled carbon nanotubes
NDs	nanodiamonds
NMR	nuclear magnetic resonance
NPs	nanoparticles
NR	nile red
PG	phytoglycogen
Ph	phenylacetyl groups
PNS	peripheral nervous system
PVD	physical vapor deposition
QELS	quasi elastic light scattering
R_g	radius of gyration

R_h	hydrodinamic radius
SAP	serum amyloid P component
SAXS	small-angle X-ray scattering
SWNT	singlewalled carbon nanotubes
TEM	transmission electron microscopy
ThT	thioflavin T
$t_{lag\ time}$	lag time
TTR	transthyretin
XPS	X-ray photoelectron spectroscopy

Abstract

The thesis deals with the testing of amyloidogenicity of various carbon nanoparticles and polymers. The first part of the thesis provides the theoretical background of amyloidoses, a group of diseases in which proteins are stored in the insoluble form of amyloid. In addition, the theoretical part also deals with a general overview of nanomaterials and the most important methods.

Several types of nanomaterials were tested within the thesis, so the part Results and Discussion was divided into two subchapters: 1) Carbon nanospecies and amyloid fibril formation, and 2) Polysaccharides, glycogen modifications and amyloid fibril formation. The first subchapter concerns the testing of four types of carbon nanoparticles (single-walled carbon nanotubes (SWNT), fullerenes (C_{60}), carbon quantum dots (CDs) and nanodiamonds (NDs)). These materials were tested on a model system hen egg white lysozyme (HEWL). Using fluorescence measurements and transmission electron microscopy (TEM), the nanoparticles were ranked from the most to the least amyloidogenic as follows: NDs> control> C_{60}> CDs> SWNT.

The second subchapter deals with the effect of selected polysaccharides (glycogen (GG), mannan (MAN), phytoglycogen (PG)) and modified GG on amyloid fibril formation. These materials were tested on the HEWL model system, as well as the amyloid beta (1-42) ($A\beta_{1-42}$) model system. The fluorescence of thioflavin T (ThT) and TEM were used to detect the growth of amyloid fibrils. In addition, fluorescence data were fitted to obtain the lag phase of the process of amyloid fibril formation. All polysaccharides accelerated the process of amyloid fibril formation from both HEWL and $A\beta_{1-42}$. In the case of modified GG, it has been shown that a small change in the structure may lead to a large change in the process of

amyloid fibril formation. Almost all GG modifications accelerated the process of amyloid fibril formation in both HEWL and $A\beta_{1-42}$, except for GG-Ph1 (1.6 mol. % phenylacetyl groups per D-glucose unit), which rather slowed down the process.

Keywords: amyloid fibrils, amyloid beta, lysozyme, polysaccharides, carbon nanoparticles

Abstrakt

Disertační práce se zabývá testováním amyloidogenicity různých uhlíkových nanočástic a polymerů. První část dizertace je věnována teoretickému úvodu týkající se amyloidóz, což je skupina nemocí, při kterých dochází k ukládání proteinů v nerozpustné formě amyloidů. Mimo to se teoretická část také zabývá obecným přehledem nanomateriálů a jsou zde také popsány nejdůležitější metody.

Vzhledem k tomu, že v práci bylo testováno více druhů materiálů, byla část věnována výsledkům a diskuzi rozdělena na dvě podkapitoly: 1) Uhlíkové nanočástice a formování amyloidních fibril, a 2) Polysacharidy, modifikace glykogenu a formování amyloidních fibril. První podkapitola se zabývá testováním čtyř druhů uhlíkových nanočástic (jednovrstvých uhlíkových nanotrubic (SWNT), fullerenů (C_{60}), uhlíkových kvantových teček (CDs) a nanodiamantů (NDs)). Tyto materiály byly testovány na modelovém systému lysozymu z vaječného bílku (HEWL). Pomocí měření fluorescence a transmisní elektronovou mikroskopií (TEM) byly testované materiály srovnány od nejvíce amyloidogeních částic po nejméně amyloidogenní následujícím způsobem: NDs> control> C_{60}> CDs> SWNT.

Druhá podkapitola se věnuje vlivu vybraných polysacharidů (glykogen (GG), mannan (MAN), fytoglykogen (PG)) a modifikací GG. Tyto materiály byly testovány nejen na HEWL, ale i na modelovém systému amyloidu beta (1-42) ($A\beta_{1-42}$). Pro detekci růstu amyloidních fibril byla použita fluorescence thioflavinu T a TEM. Data z fluorescence byla navíc fitována, pro získání délky počáteční fáze procesu tvorby amyloidních fibril. Bylo zjištěno, že všechny polysacharidy urychlily tvorbu amyloidových fibril jak z HEWL, tak z $A\beta_{1-42}$. V případě modifikací GG, bylo ukázáno, že drobná změna ve struktuře může vést

k velké změně v procesu tvorby amyloidních fibril. Téměř všechny modifikace GG zrychlily tvorbu amyloidových fibril jak v HEWL, tak v $A\beta_{1-42}$, kromě GG-Ph1 (1,6 mol. % fenylacetylových skupin na D-glukózovou jednotku), která spíše zpomalila proces ve srovnání se všemi ostatními modifikacemi.

Klíčová slova: amyloidní fibrily, amyloid beta, lysozym, polysacharidy, uhlíkové nanočástice

List of publications, a grant and contributions on conferences

Publication in journals

M. Holubová, M. Hrubý, Terapeutika amyloidóz, Chem. List. 110 (2016) 851–859. http://www.chemicke-listy.cz/docs/full/2016_12_851-859.pdf (IF = 0.39)

M. Holubova, R. Konefał, Z. Moravkova, A. Zhigunov, J. Svoboda, O. Pop-Georgievski, J. Hromadkova, O. Groborz, P. Stepanek, M. Hruby, Carbon nanospecies affecting amyloid formation, *RSC Adv.* 7 (2017) 53887–53898. https://doi.org/10.1039/c7ra11296c. (IF = 3.07)

Holubová, M., Štěpánek, P. & Hrubý, M. Polymer materials as promoters/inhibitors of amyloid fibril formation. *Colloid Polym Sci* (2020). https://doi.org/10.1007/s00396-020-04710-8 (IF = 1.536)

M. Holubová, V. Lobaz, L. Loukotová, M. Rabyk, J. Hromádkova, O. Trhlíková, Z. Pechrová, O. Groborz, P. Štěpánek, M. Hrubý, Does polysacharide glycogen behave as a promoter of amyloid fibril formation at physiologically relevant concentrations?, *Soft Matter*. (resubmitted) (IF = 3.14)

M. Holubová, V. Lobaz, L. Loukotová, M. Rabyk, J. Hromádkova, O. Trhlíková, Z. Pechrová, O. Groborz, P. Štěpánek, M. Hrubý, Chemically modified glycogens: How they influence formation of amyloid fibrils?, *Soft Matter*. (submitted) (IF = 3.14)

Chapter in a book

M. Holubová, Inorganic nanomaterials as promoters/inhibitors of amyloid fibril formation, in: C. Nardin, H. Schlaad (Eds.), Biol. Soft Matter, Wiley VCH, 2021: p. 400. (Chapter in a book, April 14, 2021)

Grant

Chemically modified glycogens as potential macromolecular therapeutics for amyloidoses (GA UK no. 386218, Monika Holubová as a main solver), year 2018 – 2020

Contributions at conferences

Holubová, M., Hrubý, M. Nanospecies affecting amyloid formation. Self-assembly in the World of Polymers. PMM Conference /80./. Prague, CR, 10-14.7.2016, Book of Abstracts and Programme. Prague: Institute of Macromolecular Chemistry AS CR, 2016. s. 139. ISBN 978-80-85009-85-9

Holubová, M., Rabyk, M., Loukotová, L., Hromádková, J., Hrubý, M., Štěpánek, P., Polymers in Medicine 2019 - Prague Meeting on Macromolecules /83./. Prague, CR, 23.-27.6.2019, Book of Abstracts and Programme. Prague: Institute of Macromolecular Chemistry, Czech Academy of Sciences, 2019. s. 96. ISBN 978-80-85009-93-4

Holubová, M., Lobaz, V., Loukotová, L., Rabyk, M., Hromádková, J., Trhlíková, O., Pechrová, Z., Groborz, O., Štěpánek, P., Hrubý, M., Does polysaccharide glycogen behave as a promoter of amyloid fibril formation at physiologically relevant concentrations? Slovensko - Česká konferencia POLYMÉRY 2020 /9./. Online 5.-8.10.2020; Book of abstract and program. Bratislava: Ústav polymérov, SAV, 2020, s. 30, ISBN 978-80-89841-14-1

1. Introduction

Amyloidoses are a group of diseases associated with the deposition of normally soluble proteins in the form of insoluble amyloids. These amyloids are deposited in various organs and tissues and cause their dysfunction and thus a major threat to human health[1,2]. The term "amyloid" was first used in botany in 1838 by Matthias Schleiden for describing plant starch, and then, in 1854, Rudolf Virchow used this term for abnormal macroscopic deposits of amyloidosis, although they had been known under various other names since the mid-seventeenth century. Virchow, using an aqueous solution of iodine and sulfuric acid, concluded that the substance, which is the base of abnormal deposits, was cellulose. The cellulosic hypothesis of amyloids did not last long. In 1859, Friedreich and Kekule demonstrated the presence of protein and the absence of carbohydrates in amyloids, which was based on a high nitrogen content[2–4]. Bennhold introduced staining with Congo red in 1922 for identification of amyloids in tissue samples[5]. In 1927, Divry and Florkin described the characteristic green birefringence when an amyloid stained with Congo red was observed in polarized light[5]. In 1959, Cohen and Calkins detected fibrillary amyloid morphology by observing it under an electron microscope[4,5]. The nature of amyloids and proteins was put together like a puzzle over the years.

However, not all amyloids are harmful. There are the so-called functional amyloids of certain proteins that are used, e.g. in mammals for melanin production[6,7], in bacteria such as *Escherichia coli* to create biofilm[7,8] etc. The high stability, organization and nanometric dimensions of amyloids make them excellent candidates for the production of nanomaterials[7] (e.g. wires, gels, scaffolds, liquid crystals, etc.) using the strategy of “bottom-up”[9]. Using amyloid fibrils as new biomaterials or finding drugs against amyloidoses requires a better

understanding of molecular mechanisms of amyloid synthesis, but also a better understanding of a number of other factors associated with amyloid formation[1].

Each protein deposition, either fibrillary or non-fibrillary, is characterized by a specific protein that is the major component of the pathological deposit. In the case of amyloidosis in humans, 36 amyloidogenic proteins are described as well as 10 more in other vertebrates where amyloid formation from the given protein is associated with a specific disease[4,10]. The current amyloid nomenclature is based on the chemical structure of the fibrillar protein and starts with the letter A (amyloid) and to it is attached a suffix that is a truncated form of the precursor protein, e.g. amyloid derived from immunoglobulin light chains is designated as AL and the disease is AL amyloidosis[4,11]. Amyloid proteins described in humans are listed in Table 1.

Some amyloidoses may be systemic (involving several organs or tissues) or localized (involving only one organ or tissue). Systemic forms of amyloidosis may be primary; sporadic or acquired forms (e.g. AL amyloidosis). In addition, systemic forms of amyloidosis may be secondary, i.e. those resulting from another disease (e.g. AA amyloidosis, see Table 1), or hereditary (e.g. ATTR amyloidosis, see Table 1). Localized forms of amyloidosis may also be sporadic or acquired (e.g. AL amyloidosis of the urinary tract and Alzheimer's disease (AD), secondary (e.g. Infectious Creutzfeldt-Jakob disease), or hereditary (e.g. many corneal dystrophies, hereditary AD)[10].

Table 1. Human amyloids and their protein precursors and target organs[4].

Amyloid	Precursor protein	Systemic (S) and/or localized (L)	Acquired (A) or hereditary (H)	Target organs
AL	Immunoglobulin light chain	S, L	A, H	All organs, usually except central nervous system (CNS)
AH	Immunoglobulin heavy chain	S, L	A	All organs except CNS
AA	(Apo) Serum amyloid A	S	A	All organs except CNS
ATTR	Transthyretin, wild type	S	A	Heart mainly in males, Lung, Ligaments, Tenosynovium
	Transthyretin, variants	S	H	peripheral nervous system (PNS), autonomic nervous system (ANS), heart, eye, leptomen.
$A\beta_2M$	β_2-Microglobulin, wild type	S	A	Musculoskeletal System
	β_2-Microglobulin, variant	S	H	ANS
AApoAI	Apolipoprotein A I, variants	S	H	Heart, liver, kidney, PNS, testis, larynx (C terminal variants), skin (C terminal variants)
AApoAII	Apolipoprotein A II, variants	S	H	Kidney
AApoAIV	Apolipoprotein A IV, wild type	S	A	Kidney medulla and systemic
AApoCII	Apolipoprotein C II, variants	S	H	Kidney
AApoCIII	Apolipoprotein C III, variants	S	H	Kidney
Agel	Gelsolin, variants	S	H	PNS, cornea
ALys	Lysozyme, variants	S	H	Kidney
ALECT2	Leukocyte Chemotactic Factor-2	S	A	Kidney, primarily
AFib	Fibrinogen α, variants	S	H	Kidney, primarily
ACys	Cystatin C, variants	S	H	PNS, skin
ABri	ABriPP, variants	S	H	CNS
ADan	ADanPP, variants	L	H	CNS
Aβ	Aβ protein precursor, wild type	L	A	CNS
	Aβ protein precursor, variant	L	H	CNS
AαSyn	α-Synuclein	L	A	CNS
ATau	Tau	L	A	CNS
APrP	Prion protein, wild type	L	A	Creutzfeldt-Jakob disease (CJD), fatal insomnia
	Prion protein variants	L	H	CJD, Gerstmann–Sträussler–Scheinker (GSS) syndrome, fatal insomnia
	Prion protein variant	S	H	PNS
ACal	(Pro)calcitonin	L	A	C-cell thyroid tumors
AIAPP	Islet amyloid polypeptide	L	A	Islets of Langerhans, insulinomas
AANF	Atrial natriuretic factor	L	A	Cardiac atria
APro	Prolactin	L	A	Pituitary prolactinomas, aging pituitary
AIns	Insulin	L	A	Iatrogenic, local injection
ASPC	Lung surfactant protein	L	A	Lung
AGal7	Galectin 7	L	A	Skin
ACor	Corneodesmosin	L	A	Cornified epithelia, hair follicles
AMed	Lactadherin	L	A	Senile aortic media
AKer	Kerato-epithelin	L	A	Cornea, hereditary
ALac	Lactoferrin	L	A	Cornea
AOAAP	Odontogenic ameloblast-associated protein	L	A	Odontogenic tumors
ASem1	Semenogelin 1	L	A	Vesicula seminalis
AEnf	Enfurvitide	L	A	Iatrogenic
ACatK	Cathepsin K	L	A	Tumor associated

1.1. Amyloid

All amyloids share several physicochemical properties: fibrillary morphology, secondary structure of the β-sheet, an apple green birefringence after dyeing with Congo red, insolubility in common solvents and detergents, and resistance to proteases. The amino acid sequence and structure of proteins associated with amyloidosis are highly variable[12,13]. Amyloids have cytotoxic effects such as induced failure of autophagy, increased levels of reactive oxygen species (ROS), mitochondrial dysfunction, cell membrane penetration, calcium dyshomeostasis, or loss of protein function after aggregation[14,15].

1.1.1. Amyloid fibrils

Amyloid fibrils are a major component of amyloids and are formed from a specific (amyloidogenic) protein[4]. Some amyloidogenic proteins in their soluble states have a globular structure (e.g. transthyretin (TTR)). It was shown that these proteins must be partially unfolded to produce fibrils. In these cases, most amyloidogenic mutations destabilize the globular structure, thereby increasing the steady-state concentration of partially unfolded globular proteins and promoting fibril formation. The proteins that are not amyloidogenic *in vivo* have been shown to be able to induce fibril formation when the protein is exposed to partial denaturation conditions that mimic the effect of a destabilizing mutation. This suggests that the ability to produce fibrils is a general feature shared by many proteins and only occurs under conditions of partial denaturation. Unlike globular proteins, many amyloidogenic proteins in their native soluble state occur in the form of a random coil. These proteins may possess a metastable conformation which needs to have an optimal α-helix content to prefer a transition from a random coil to a β-sheet during the fibrillation[16].

Amyloid fibrils have variable length and they are rigid and non-branched with 7-12 nm diameter[17,18]. Amyloid fibrils are composed of at least two fibrous subunits, which are called protofilaments and rotate along the fibril axis[13]. Protofilaments have a diameter of 2.5 to 3.5 nm and consist of a number of anti-parallel β-sheets, which slowly turn along the axis of protofilaments and form a helical structure[17,19]. The basic unit of the β-sheet is the β-strand which is a part of the polypeptide chain and is perpendicular to the protofilament axis[14]. This structure is called cross-β[20]. Figure 1 shows a scheme of the individual amyloid subunits.

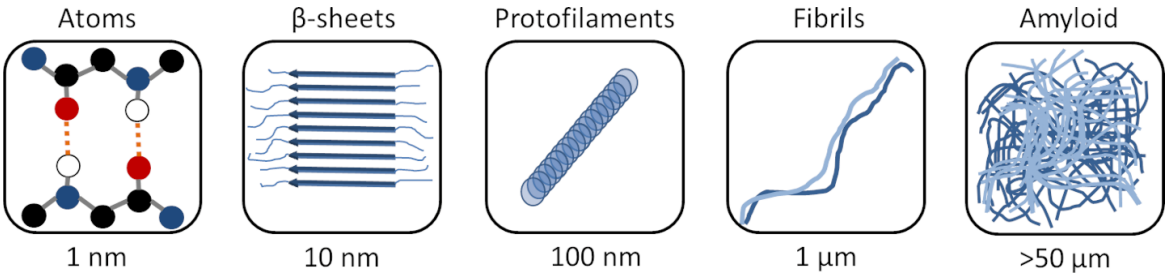

Figure 1. Subunits of amyloids

Amyloid fibril formation usually includes a combination of several factors such as increased and long-term distribution of the protein and/or the susceptibility of the protein to form the structure of a β-sheet, which may be due to mutation and denaturing conditions. This property can also be obtained during proteolytic cleavage[11]. Counterparts of amyloidogenic proteins are synthesized and secreted as native proteins, but the intracellular control system is normally able to detect and remove them. Fluctuation of the concentration of both forms is high. There are a number of factors that can shift the balance towards partially unfolded forms of protein, such as low pH, oxidation, increasing temperature or metal ions[21]. Generally, amyloid formation occurs due to oligomerization of nuclei which also accelerate amyloid formation. After nucleation, the fibrils start growing rapidly. Some cases of the formation of amyloid fibrils may require proteolysis that leads to the release of

an amyloidogenic protein. In this case, they are called fragments of the precursor protein (fibrillogenic peptide). Generally, the sensitivity of the proteolytic precursor to produce fragments for formation of amyloid fibrils is due to a mutation, this mutation is necessary for cleavage of the protein *in vivo*[16].

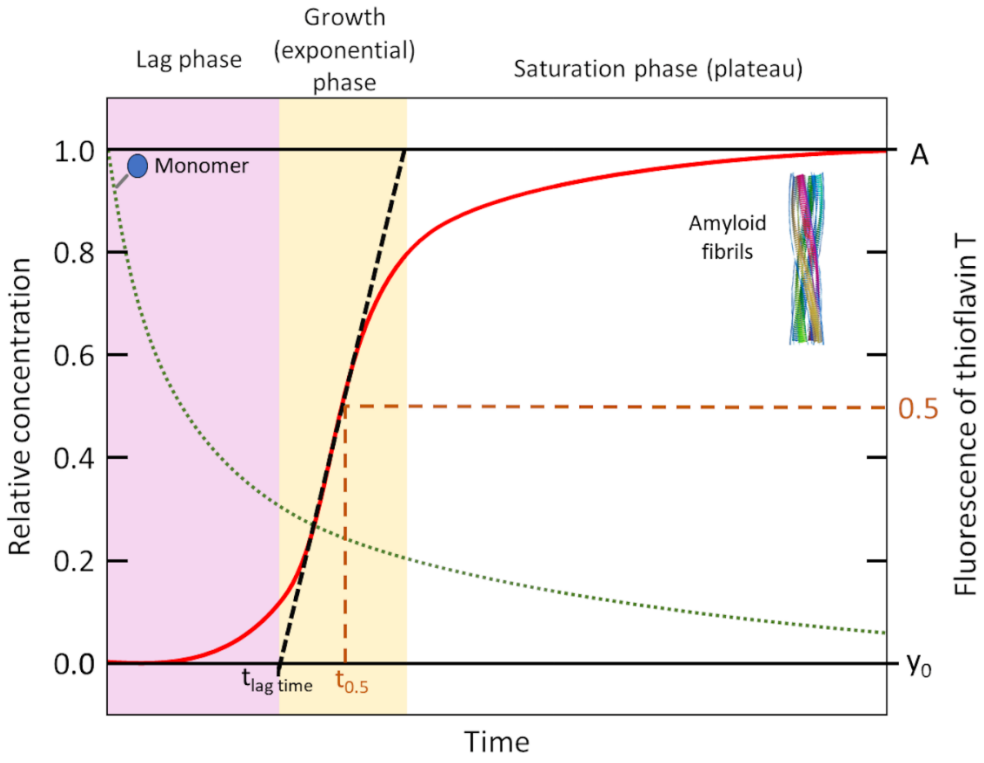

Figure 2. Scheme of the sigmoidal increase in thioflavin T (ThT) fluorescence/protein concentration in amyloid forms (red line) during the process of amyloid fibril formation. The green dotted line represents the monomer concentration (soluble amyloid protein). Adapted from ref.[22]. The black dashed line corresponds to the slope of the growth phase. The time $t_{0.5}$ corresponds to the time at which 50% of the maximal fluorescence is observed. The y_0 line is the initial baseline, and A is the amplitude of fluorescence[23]

The formation of amyloid fibrils is a very complex process. The growth of amyloid fibrils traces a sigmoidal curve of fluorescence thioflavin T (ThT)[24] that is used for a rapid detection of amyloid fibrils. The same curve also describes the protein concentration in amyloid forms. An example of such a curve is shown in Figure 2 (red line)[25,26]Based on this curve, we can estimate phases of the process of amyloid fibril formation. The process of

amyloid fibril formation includes three phases: 1) the lag phase, when soluble proteins create nuclei that form oligomeric species with β-sheets; 2) the growth phase, when fibril elongation occurs; and 3) the saturation phase, when mature fibrils are finalized[12]. Amyloid fibril formation includes a number of intermediate states and pathways[22,27]. As mentioned, fibril formation can be described by a sigmoid curve (red line in Figure 2), which means that the measured data can be fitted with a sigmoidal curve, that can be described by the following equation (1)[23,25,26]:

$$Y(t) = y_0 + \frac{A}{1 + exp\,(-k(t - t_{0.5}))} \quad (1)$$

where t is time, $Y(t)$ is fluorescence intensity, y_0 is the initial baseline, A is the amplitude of fluorescence, $t_{0.5}$ is the time at 50% maximal fluorescence, and k is the apparent growth rate. The lag time ($t_{lag\ time}$) was defined according to equation (2)[23,25,26].

$$t_{lag\ time} = t_{0.5} - \frac{2}{k} \quad (2)$$

This definition of lag time corresponds to the extrapolation from the maximal growth rate to the intercept with the baseline (Figure 2)[23,25,26].

In order to study the process of fibrillation, short peptides are usually used because of simplification, because fibrillation is a very complex process. It has been shown that even relatively short peptides, which are certain fragments of a precursor protein, have the ability to generate typical amyloid fibrils. The small size of the peptides reduces the complexity of amyloid formation and at the same time allows us to obtain a physicochemical view of the mechanism of fibril formation. A typical common feature of short peptides that can form amyloid fibrils is a high occurrence of aromatic amino acid residues[28]. The importance of aromatic rings in the formation of amyloids has been demonstrated in many peptides. In

addition, these interactions are important in many areas of structural biology, including the formation of hydrophobic nuclei of proteins conferring the stability of the tertiary structure, "host-guest" interaction, aggregation of porphyrins in solution, and nucleobases stabilization[29]. The proposed role of aromatic interactions in fibril formation is related to the finding that the amyloid fibril structure resembles a β-helical structure where one or more β-sheets are helically twisted around the nucleus[30]. One of the main properties of a β-helix is the layering of similar residues on a flat β-sheet.

Other important interactions for aggregation and stabilization of amyloid fibrils are hydrophobic[31] interactions. The substitution of an amino acid in a sequence that plays a key role in the behaviour of the whole sequence may reduce (or increase) the tendency to aggregation while reducing (or increasing) hydrophobicity[31,32]. There is evidence that protein sequences have evolved to prevent clusters of hydrophobic residues (e.g. groups of three or more consecutive hydrophobic residues are less common in protein sequences[32]). Aggregation and stabilization are also affected by electrostatic interactions[31,32]. In cases where the protein is highly charged, aggregation of proteins is energetically unfavourable. If proteins have positively and negatively charged groups on the surface, it can lead to aggregation[31,33].

1.1.2. Other species contained in amyloids

In addition to the precursor protein, serum amyloid P component (SAP)[17], glycosaminoglycans[17] (mainly heparan sulfate) and apolipoprotein E (APOE)[34] have been found in amyloids of various amyloidosis[17,21]. The non-fibrillar form of SAP is a pentameric globular glycoprotein that binds reversibly to amyloid fibrils depending on Ca^{2+} concentration and is a universal component of amyloids. SAP forms 12 % to 20 % of amyloid

dry matter. SAP is a normal plasma protein that is produced in the liver together with a C-reactive protein. SAP is a key component of innate immunity and inflammation and can also form amyloid fibrils, causing secondary amyloidosis resulting from inflammation. The non-fibrillar form of SAP is very readily associated with amyloid fibrils. The main role of SAP is preventing the degradation of amyloid fibrils by proteolytic enzymes.

Glycosaminoglycans (GAGs) have been shown to promote aggregation of amyloidogenic proteins. GAGs as polyanions play an important role in catalysing protein aggregation and stabilizing amyloid fibrils[17]. GAGs are long, unbranched linear polymers, that consist of repeated disaccharide units. Most of GAGs are sulfated (e.g., heparan sulfate is largely composed of iduronic acid and *N*-acetylglucosamine-(4/6/2)-sulfate) only hyaluronic acid is a nonsulfated GAG[35]. The GAGs accelerate the process of amyloid fibril formation[36,37]. On the other hand, the acceleration of amyloid fibrils reduces the concentration of oligomer species with a higher cell toxicity than mature amyloid fibrils[38]. There is a theory that GAGs behave as other polyanions that are also able to promote the aggregation of amyloid fibrils. However, the exact role and interaction of these components is not well known[17].

The role of APOE is not well known in the pathogenesis of amyloids[17]. There are three major polymorphisms of APOE in the human gene: ε2, ε3 and ε4. The last mentioned ε4 is associated with an increased risk of developing AD[34]. It is known that APOE has a key role in the process of amyloid fibril formation mainly in conversion from protofibrils to fibrils and it depends on an isoform[34].

1.2. Nanospecies

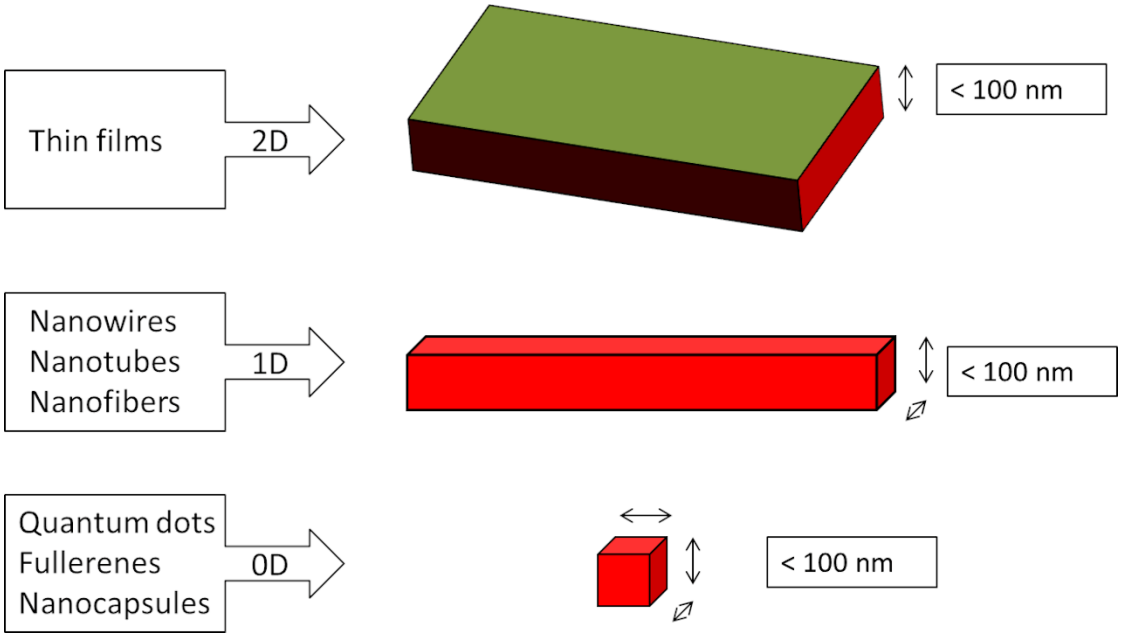

Figure 3. Classification of nanomaterials.

Nanotechnology is a broad term for technologies implemented at the nanoscale with real-world application[39]. Nanotechnology has penetrated a wide range of fields, e.g. physics, chemistry, biology, material science, health sciences, and engineering[40]. We can divide materials used in nanotechnology to "zero-dimensional" (0D), "one-dimensional" (1D) and "two-dimensional" (2D) objects. Figure 3 shows the above-mentioned classification of nanomaterials. When we talk about 0D nanomaterials, we mean nanoparticles (NPs)[41,42] of various shapes (e.g., quantum dots, dendrimers, nanocapsules, and fullerenes)[42]. In case of 1D nanomaterials, one dimension is out of the nanoscale (e.g. nanowires, nanotubes and nanofibres). The last category, 2D nanomaterials, have even two dimensions outside the nanoscale (e.g., thin films)[41,42].

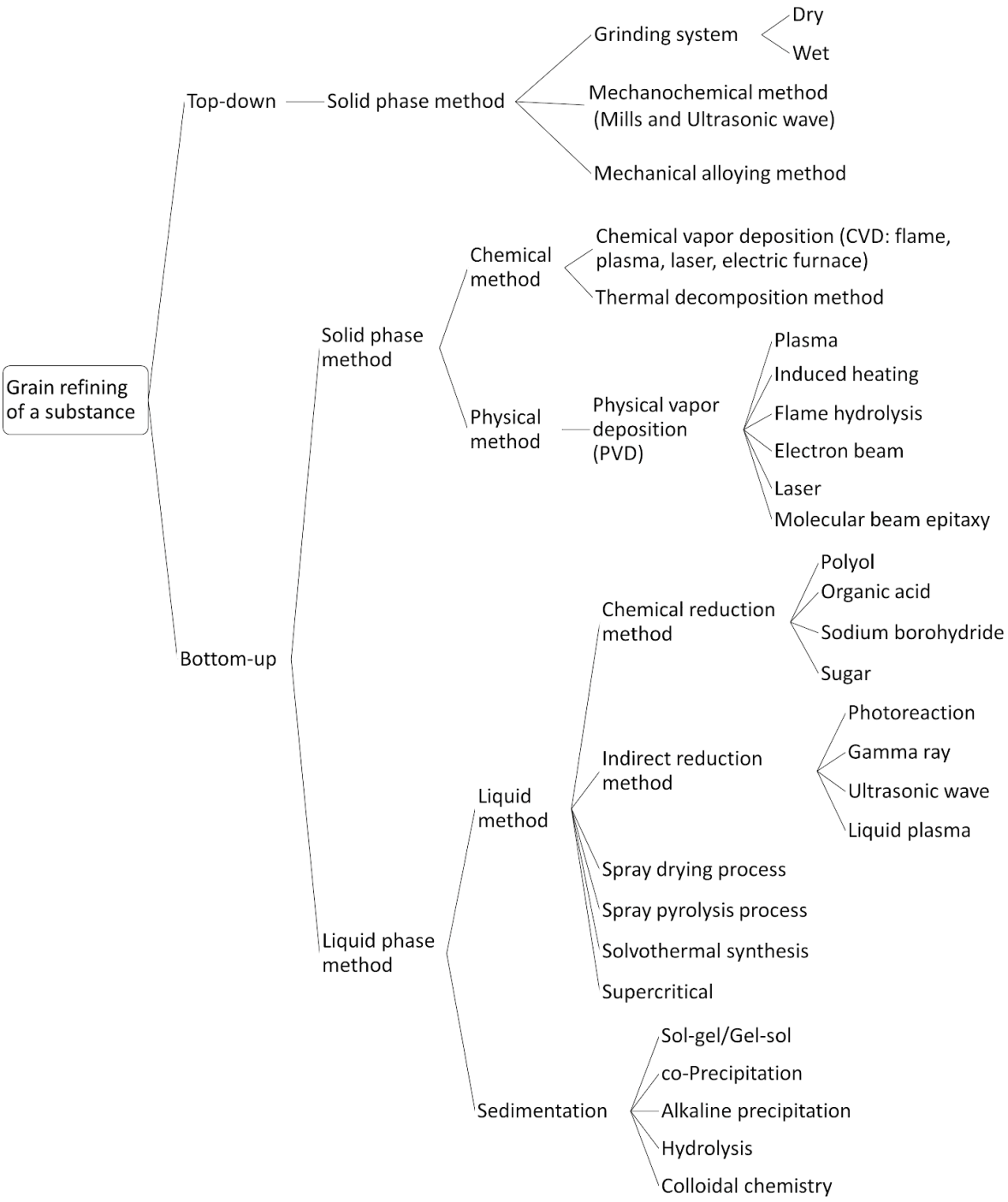

Figure 4. Different methods for the preparation of nanomaterials. Adapted from ref.[43]

There are two main methods of producing nanomaterials. These are the so-called "top-down" and "bottom-up" methods. In case of "top-down" approaches, it is necessary to use an external force that is applied to a bulk material resulting in the formation of a

nanomaterial[42,43]. However, more advantageous methods for preparation of nanomaterials are "bottom-up" approaches, because it is easier to control the shape, structure, and size during synthesis[44] as the nanomaterials are assembled from molecules or nanoclusters based on atomic transformations or molecular condensations[42,43]. A number of different methods used for the preparation of nanomaterials are shown in Figure 4.

Nanomaterials have many unique properties and are therefore used in a wide range of applications, for example in medicinal and pharmaceutical areas including biosensing, diagnostics, and drug delivery, or nanoelectronics systems with implants[44–46]. Nanomaterials can be applied not only in medicine, but also in environment protection as monitoring devices (nano-biosensors), catalysts, water cleaning and purification (filtering membrane technologies), nano-based photocatalytic processes of semiconductor materials (titanium dioxide (TiO_2), air cleaning and purification, soil remediation (e.g., using iron nanoparticles), etc.[46] Many areas of industry, such as automotive, construction, aerospace, textiles, sports, etc., also use nanomaterials[46]. They are used in the automotive industry as a dispersion part in composites to improve the required properties of the matrix[47]. Nanomaterials are also used in coatings and paints to achieve surfaces with special properties, e.g. antimicrobial surfaces, anti-scratch paints, etc.[46,47] We must not forget to mention electronic components, where nanomaterials are widely used today[46,47].

As mentioned some applications of nanomaterials are beneficial to the environment (e.g. water or air purification[48]) or human health (drug delivery systems[49]). Today, nanomaterials are everywhere and they are contained in more than 800 products such as cosmetics, cigarette filters, antimicrobial and stain-resistant fabrics, sprays and sunscreens[45]. Although they help us today in a number of sectors, it is also necessary to address their risks. The biggest problem is their unique properties, which include a large surface area to mass

ratio, which is associated with increased surface reactivity to make such materials potential contaminants, which may endanger human health[45]. Potential pathways of nanomaterials are shown in Figure 5.

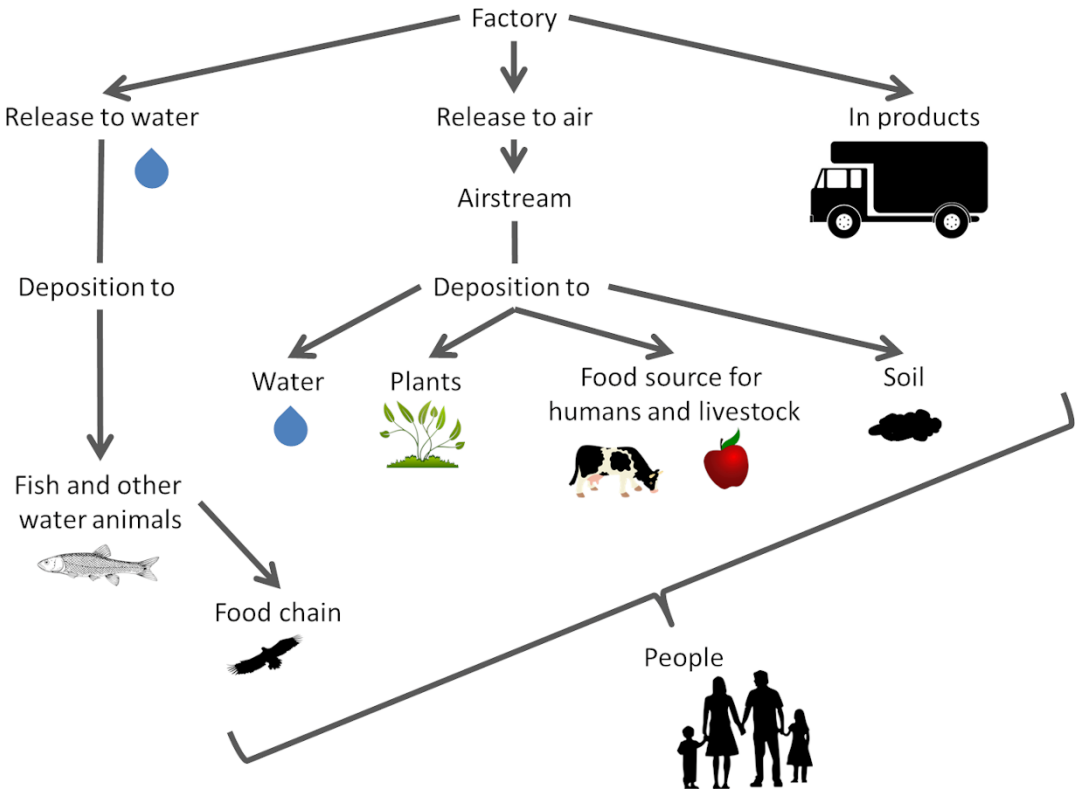

Figure 5. Pathways of nanomaterials exposure[48].

2. Methods

2.1. Dynamic light scattering

Dynamic light scattering (DLS), sometimes also called quasi elastic light scattering (QELS), is a very useful method for measuring the size and size distribution of molecules and particles in the nanoscale region. DLS is very often used for characterization of particles, emulsions or molecules which have been dispersed or dissolved in a liquid. The Brownian motion of particles or molecules in suspension causes laser light to be scattered at different

intensities. The motion of particles can be analyzed using intensity correlation function $g^{(2)}(t)$ which is related to the field correlation function $g^{(1)}(t)$ by the Siegert relation[50,51],

$$g^{(2)}(t) = 1 + \beta\left|g^{(1)}(t)\right|^2 \quad (3)$$

where t is the delay time of the correlation function and β is an instrumental parameter. The distribution of relaxation times $A(\tau)$ of scattered light can be modeled by the Laplace transformation, according to the equation[50,51]:

$$g^{(1)}(t) = \int A(\tau)(\exp(-t/\tau))\, d\tau \quad (4)$$

After performing the inverse Laplace transformation, we get $A(\tau)$ from $g^{(1)}(t)$. The relaxation time τ is linked to the diffusion coefficient D, using the equation[50,51];

$$D = \frac{1}{\tau q^2} \quad (5)$$

where q is the scattering vector. Using the Stokes-Einstein equation (eq. 6) it is possible to calculate the hydrodynamic radius R_h of particles[50]:

$$D = \frac{k_B T}{6\pi\eta R_h} \quad (6)$$

where k_B is the Boltzmann constant, T is absolute temperature and η is the viscosity of the solvent.

2.2. Electrophoretic light scattering

Electrophoretic light scattering (ELS) is a technique used to measure the ζ-potential. The ζ-potential is the potential difference at the slipping plane, which is established during the relative motion of the solid phase with the electric bilayer to the solution. The ζ-potential measurement is based on the principle of electrophoresis. Electrophoresis is the movement of a charged particle relative to the liquid it is suspended in under the influence of an applied

electric field[52]. The Henry equation (7) describes the relationship between the electrophoretic mobility and ζ-potential:

$$U_e = \frac{2\varepsilon\zeta F(ka)}{3\eta} \quad (7)$$

where U_e is the electrophoretic mobility, ζ is the ζ-potential, ε is the dielectric constant, η is the viscosity of the solvent and *F(ka)* is Henry's function[52].

2.3. Techniques for monitoring of amyloid fibril formation – *in vitro*

Among the most commonly used techniques for monitoring amyloid fibril formation are fluorescence of thioflavin T (ThT) and transmission electron microscopy (TEM). Another technique which can be used is circular dichroism, which is very useful for studying the comparison to native conformation, the structural changes that accompany the association/dissociation of ligands and also during the unfolding/refolding of biomolecules[53]. It is also possible to find studies which use Fourier transform infrared spectroscopy (FTIR)[54,55] or atomic force microscopy (AFM)[54].

2.3.1. Transmission electron microscopy

A widely used technique for imaging amyloid fibrils is TEM. A simple scheme of TEM is shown in Figure 6. Generally, TEM works in the following way: An electron gun, where cathode is a source of electrons, in a form of heated V-shaped tungsten filament or a rod of lanthanum hexaboride (LaB_6), produces the electron beam that irradiates a thin specimen. The electron energy is usually 60-150 keV (the most used is 100 keV). The distribution of electron intensity behind the specimen is imaged with a lens system, onto a fluorescent screen. Using TEM, it is possible to achieve a resolution of the order of 0.2-0.5 nm[56–58]. Therefore, it is not a problem to display amyloid fibrils with a diameter of approximately 7-12 nm. TEM micrographs can be used for a qualitative comparison of fibrils,

in particular the curvature of fibrils, the smoothness of their surface, etc. On the other hand, TEM is also used for a quantitative analysis, which includes, e.g. the length of early aggregates and seeds, the width of fibrils, etc.[59] A big advantage is that it is a very fast method and tells us the immediate morphology of the sample. The problem is that it only shows the morphology of samples (fibrils or other structures). Whether visible fibrils are amyloid fibrils that contain a cross-β structure, must be confirmed by another method. Negative staining, e.g. uranyl acetate[59], is used for a better contrast of samples with amyloid fibrils. Negative staining preserves well the morphology of a sample and, in addition, protects the specimen from radiation damage[59].

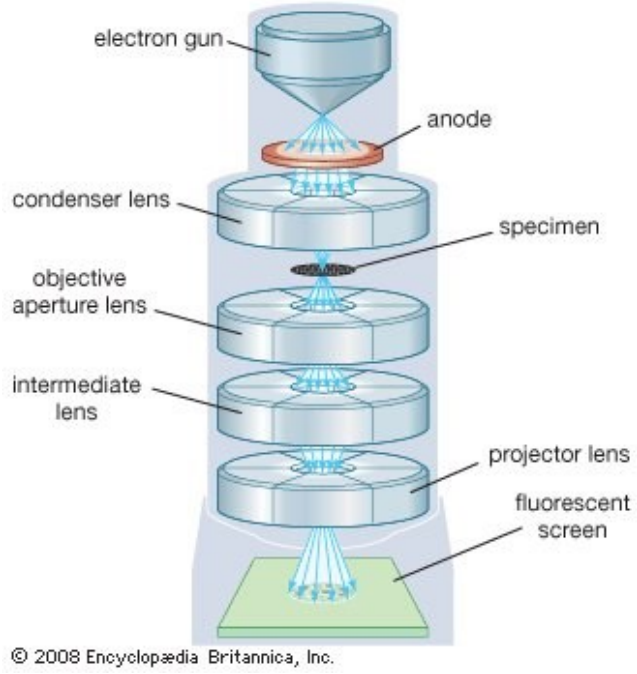

Figure 6. Scheme of TEM[58].

2.3.2. Fluorescence of thioflavin T

Thioflavin T (ThT) is the most common probe using *in vitro* monitoring of amyloid fibril formation. A structure of ThT is shown in Figure 7. ThT has a hydrophobic part

containing a dimethylamino group attached to a phenyl group. The hydrophobic part is connected to a more polar benzothiazole group containing the polar N and S[24,60–62].

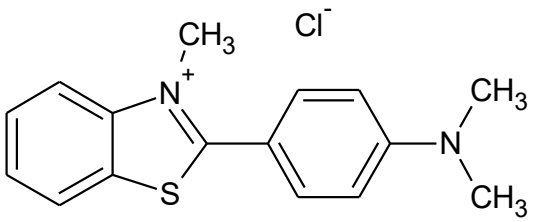

Figure 7. Thioflavin T.

ThT can form micelles in aqueous solution. ThT binds specifically to amyloid fibrils, leading to an increase in the fluorescence signal at approximately 482 nm when it is excited at 450 nm[24,60–62]. The increase in fluorescence upon binding to amyloid fibrils is caused by rotational immobilization of the central C–C bond, that connects the benzothiazole and aniline rings[63]. Due to the fact, that ThT is a charged molecule, its binding properties to amyloid fibrils are dependent on the pH. In general the intensity of ThT fluorescence is up to 10 times decreased in acidic pH[64]. Therefore, it is necessary to find a compromise between the protein/peptide concentration, pH of the environment, etc.

2.3.3. Isothermal titration calorimetry

Isothermal titration calorimetry (ITC) is a very useful technique for monitoring binding affinities. ITC is the best choice for monitoring the interaction between biological macromolecules[65]. ITC directly measures the energy that is associated with a certain chemical response after mixing two components. In a typical ITC experiment, one component is gradually added (in 10 μL steps) to the other component in a reaction cell (~1 mL). ITC measures the heat production or absorption when the molecules of both components interact with each other. When a certain amount of the other component is

injected into a calorimeter cell containing one component, heat (q_i) is proportional to the amount of ligand released or absorbed. The chemical reaction is characterized by binding enthalpy (ΔH):

$$q_i = v \times \Delta H \times \Delta L_i \quad (7)$$

where v is the volume of the reaction cell and ΔL_i is the increase in the concentration of bound ligand after the i^{th} injection. Modern ITC devices work on the principle of heat compensation. The measured signal depends on the amount of energy necessary to maintain a constant temperature difference between the reaction and reference cells. The second component can be injected gradually or continuously. From the raw values it is possible to determine all the important thermodynamic data on the reaction, such as ΔH, binding entropy (ΔS) and binding free energy (ΔG). Other reaction parameters can also be determined using the software of the respective devices. Thanks to their high sensitivity and small reaction vessel, these devices are very suitable for biomolecular and pharmaceutical purposes[66,67].

3. Aims of the thesis

The main goal was to test a series of nanospecies using the proposed model fibrillation systems. The individual specific aims were as follows:

1. Design and fine-tune a model protein or peptide system for testing amyloidogenicity
2. Investigate and compare the influence of selected carbon nanospecies on the process of amyloid fibril formation
3. Investigate the influence of selected polysaccharides and several modifications of polysaccharides on the process of amyloid fibril formation.

4. Results and discussion

The main task was to test several types of nanospecies and evaluate their influence on the process of amyloid fibril formation. We investigated nanospieces from three groups of materials and, therefore, this part was divided into two subchapters: 1) Carbon nanospecies and amyloid fibril formation, and 2) Polysaccharides, glycogen modifications and amyloid fibril formation. A positive control (model protein/peptide systems) was always used for the experiments, which means that the amyloid fibrils were always created in the control. An acceleration/slowing down or inhibition of the process of fibrillation could be observed from the performed experiments. For all groups, hen egg-white lysozyme (HEWL) was used, designed as a model system for both groups of materials. HEWL is a small protein with four disulfide bonds[68] which has been studied as a model of the human lysozyme[69], whose mutation (sharing 60 % of its sequence identity with HEWL) is associated with hereditary systemic amyloidosis[70]. We also used another model system for testing, amyloid beta (1-42) ($A\beta_{1-42}$). Aβ peptide is created when amyloid precursor protein (APP) is cleaved by amyloidogenic pathway. The size of Aβ can range from 38 to 43 amino acids depending on the cleavage site on the precursor protein. There are common isoforms $A\beta_{1-40}$ (90%) and $A\beta_{1-42}$ (10%). $A\beta_{1-42}$ is the most fibrillogenic form[71]. Although the physiological concentration of Aβ is important for normal memory function and synaptic plasticity[72], Aβ in a high concentration forms amyloid fibrils in senile plaques that cause neurotoxicity and cell death. These senile plaques are associated with Alzheimer's disease[71–73]. In almost all the experiments, ThT fluorescence was used for a rapid detection of amyloid fibril formation. The results from fluorescence were always supported with TEM, which is the most suitable and fastest technique for checking morphology.

4.1. Carbon nanospecies and amyloid fibrils formation

Carbon nanospecies (CNPs) such as fullerenes (C_{60}), carbon quantum dots (CDs), single- (SWNT) and multiwalled carbon nanotubes (MWNT), or nanodiamonds (NDs), have many unique properties, and therefore are useful in many areas. These nanomaterials are produced not only by high-tech methods, but also by common processes (Figure 8) such as the burning and pyrolysis of organic materials, arc discharge welding and explosions. It is the reason why CNPs may occur in nature and become potential contaminants[74]. CNPs may catalyze protein misfolding and subsequent amyloid fibril formation, which are connected with the group of diseases called amyloidoses. The focus was on testing and comparing several selected CNPs (SWNT, C_{60}, NDs and CDs).

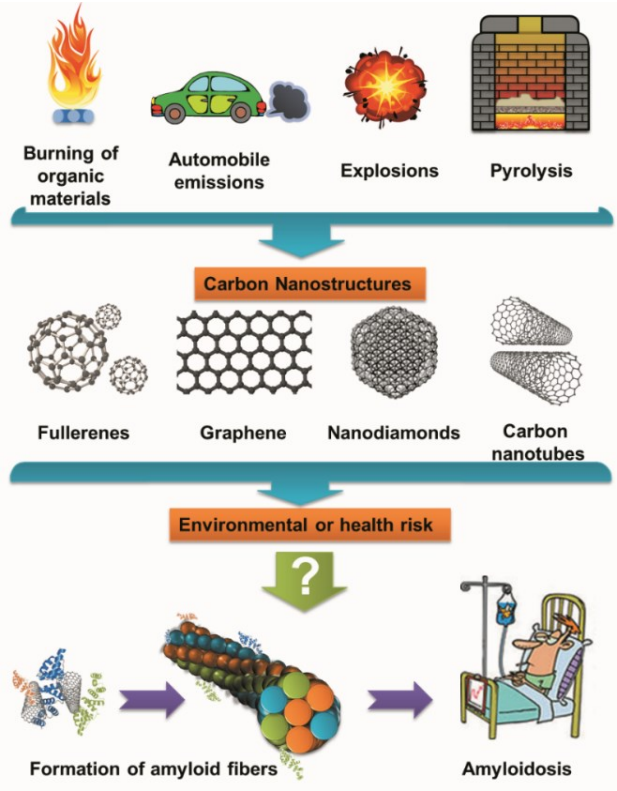

Figure 8. Potential paths of CNPs in environment.

4.1.1. Characterization of CNPs

SWNT, C_{60}, ND and CDs were commercial materials, therefore, a brief characterization was performed on them. The situation was different with the CDs that were synthesized from citric acid and urea.

Carbon quantum dots (CDs)

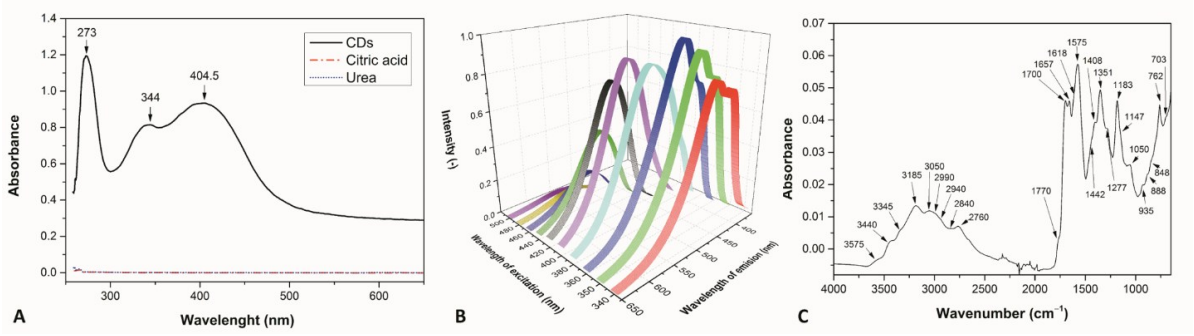

Figure 9. (A) UV-Vis absorption spectrum, (B) PL spectra at various excitation wavelengths and (C) FTIR spectrum of the CDs.

A diluted solution of CDs had a light-yellow color. The light-yellow solution of CDs showed blue emission under a UV lamp with a wavelength of 366 nm. The ζ-potential of the CDs was measured as -31.2 mV. UV-vis absorption showed a broad absorption spectrum with maxima at 273 nm, 344 nm and 404.5 nm (Figure 9A). It was shown, that CDs had excitation-wavelength-dependent photoluminescence properties, wherein the strongest fluorescence emission band at 460 nm was observed for 360 nm excitation (Figure 9B).

The composition of CDs was examined by elemental analysis (EA), FTIR spectroscopy (Figure 9C), X-ray photoelectron spectroscopy (XPS) (Figure 10) and nuclear magnetic resonance (NMR) spectroscopy (Figure 11). EA revealed the composition of the CDs to be C 41.94 wt. %, H 4.33 wt. %, N 19.36 wt. % and O (calculated) 34.38 wt. %. All other methods were in very good agreement, because they confirmed that CDs contained a

mixture of functional groups. Even XPS and EA showed similar values for the individual elements (Table 2).

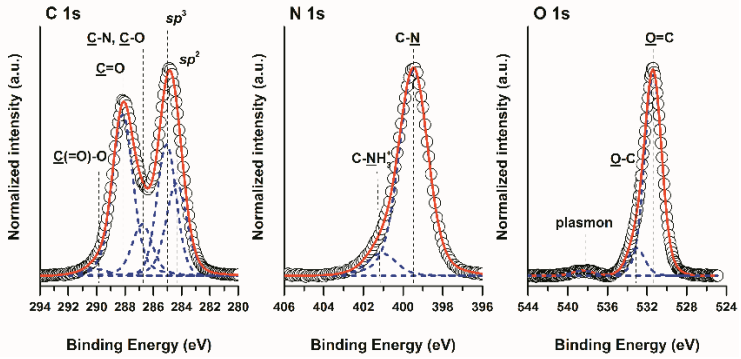

Figure 10. High-resolution C 1s, N 1s and O 1s XPS spectra of CDs. Measured spectra are indicated by black circles and their corresponding fits of data are represented by red lines. The individual contributions of different functional groups present in the CDs are represented by blue lines.

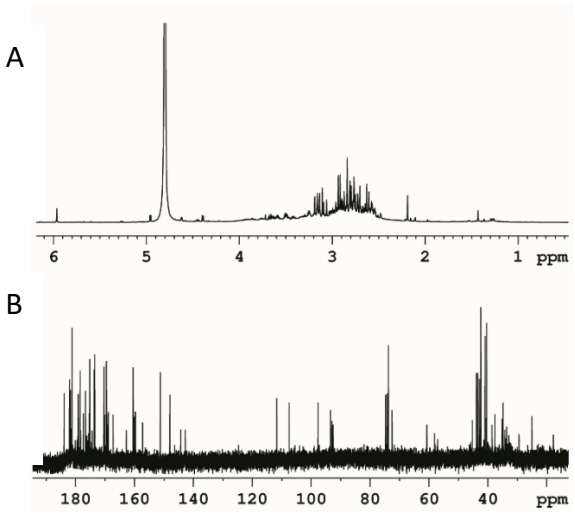

Figure 11. ^{1}H NMR (A) and ^{13}C NMR spectra (B) of the CDs in a D_2O solution.

The last method used for characterization of CDs was Small-angle X-ray scattering (SAXS). Using SAXS it was found, that CDs had a radius of gyration (R_g) approximately 6.8 Å. For the calculation of the molecular weight (M_w), it was assumed that the CDs are spherical and their density was estimated to 1.3 g/cm^3. Based on these assumptions, M_w of CDs was 1817 g/mol.

Table 2. The composition of CDs determined by XPS and EA.

	Functionality	***XPS individual contributions [wt. %]***	***XPS total [wt. %]***	***EA [wt. %]***
C	C=C	10.1±1.3	50.1±0.8	43.9±0.1
	C—C	14.4±1.2		
	C—N, C—O	6.2±0.1		
	C=O	18.5±0.4		
	C(=O)—O	0.9±0.2		
N	C—N	17.7±0.5	19.9±0.6	20.2±0.1
	C—NH_3^+	2.2±0.3		
O	O=C	27.1±0.5	30.0±0.3	35.9±0.1
	O—C	2.9±0.4		

SWNT, C_{60} and ND

SWNT, C_{60} and NDs were characterized with DLS and TEM. Additionally, NDs were also measured using FTIR and Raman spectroscopy to determine the surface group and confirm a diamond structure. The values of R_h are shown in Table 3 and TEM micrographs are shown in Figure 12. Because SWNT and C_{60} did not have surface stabilization, they formed large clusters, that were observed with both DLS and TEM. The SWNT clusters had R_h = 120±16 nm; however, the aspect ratio of carbon nanotubes must be taken into account. It was confirmed with TEM, because TEM micrograph of SWNT showed very long tangled nanotubes (Figure 12A). The C_{60} clusters (Figure 12B) were similar to clusters described in literature[75,76]. NDs were stabilized in suspension, but DLS measuring also showed clusters, although individual NDs predominated. This was also confirmed with TEM (Figure 12B). For NDs, we also measured the ζ-potential because it is very important in interaction with proteins. Unlike CDs, NDs had a positive ζ-potential +45±3 mV.

Table 3. The values of R_h of CNPs.

CNPs	***Intensity R_h***
SWNT	120±16 nm (clusters)
C_{60}	373±86 nm (clusters)
NDs	66±3 nm (clusters)
	13±5 nm (individual)

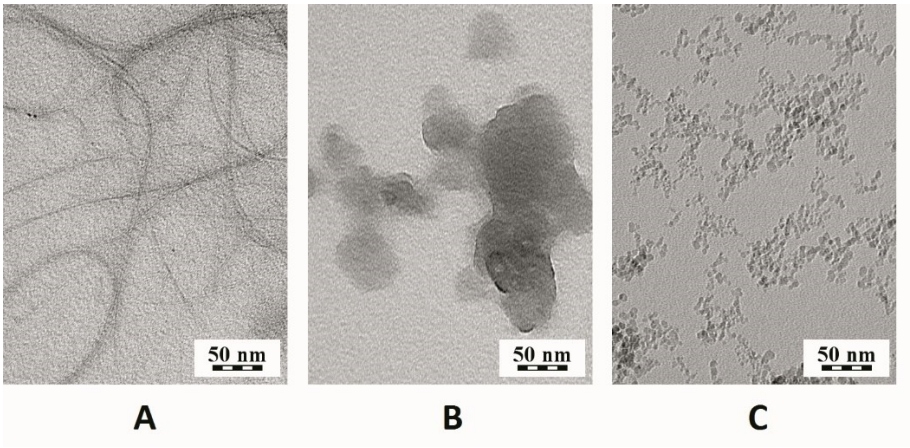

Figure 12. TEM micrographs for (A) SWNT; (B) C_{60} and (C) NDs.

4.1.2. Characterization of amyloid fibril formation in the presence of CNPs

To determine amyloid fibril growth, ThT fluorescence and TEM was used. in case of CDs, there was a problem with using ThT for monitoring because the spectra of ThT and CDs overlap. Therefore, a different dye, Nile red (NR), was chosen for monitoring amyloid fibril formation. NR can also be used for monitoring amyloid fibril formation. NR is an uncharged, heterocyclic fluorescence dye (Figure 13)[77] that has a high affinity to amyloid fibrils and whose fluorescence increases after binding to mature fibrils[78].

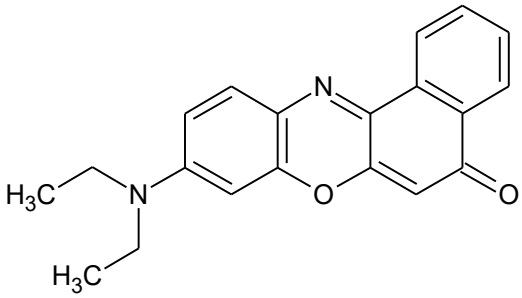

Figure 13. Structure of nile red

Figure 14 shows graphs of ThT fluorescence for experiments with the control (only HEWL) and HEWL with different concentration of SWNT, C_{60} and NDs. The graph in Figure 14A shows that the highest concentration of C_{60} (250 µg/mL) accelerated the fibrillation process, while both lower concentrations of C_{60} (16 and 80 µg/mL) show a statistically significant deceleration of the process of amyloid fibril formation. However, TEM micrographs of all samples with C_{60} (Figure 15E-G) show the typically long amyloid fibers similar to the control (Figure 15A). TEM micrographs also show some spherical particles, but these are probably artifacts that occurred during the sample preparation.

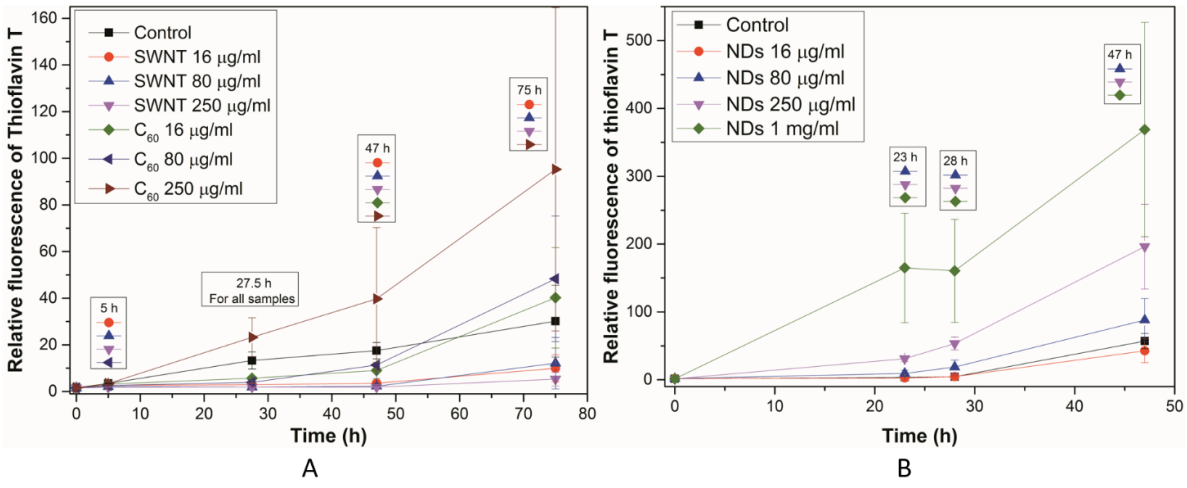

Figure 14. Graphs of the relative fluorescence of thioflavin T in experiments with (A) SWNT and C_{60}; (B) NDs. The legend above the results from the same time represents a statistically significant difference ($\alpha<0.05$) when compared to a control at same time

In case of SWNT, we observed a strong slowing down of the process of amyloid fibril formation (Figure 14A). It was also supported by TEM micrographs of samples with SWNT (Figure 15B-D). In case of 16 μg/mL concentration SWNT (Figure 15B), long mature fibers were observed similar to the control (Figure 15A). The TEM micrograph of a higher concentration (80 μg/mL SWNT) showed long fibrils, but also shorter fibrils (Figure 15C). The strongest effect was observed for the highest concentration (250 μg/mL SWNT, Figure 15D). There we observed a different morphology than that of the control. TEM micrographs reveal a fibrillary morphology, but not typically amyloid fibrils, because the formed fibrils in the presence of SWNT are thicker than amyloid fibrils. The surface of SWNT probably terminated the formation of amyloid fibrils.

Results for NDs are different than for C_{60} and SWNT. NDs in almost all concentrations, except 16 μg/mL, accelerated the process of amyloid fibril formation (Figure 14B). NDs behaved like efficient amyloid fibrillation initiators. The TEM micrographs of all ND samples (Figure 16B-D) show long fibers similar to the control (Figure 16A).

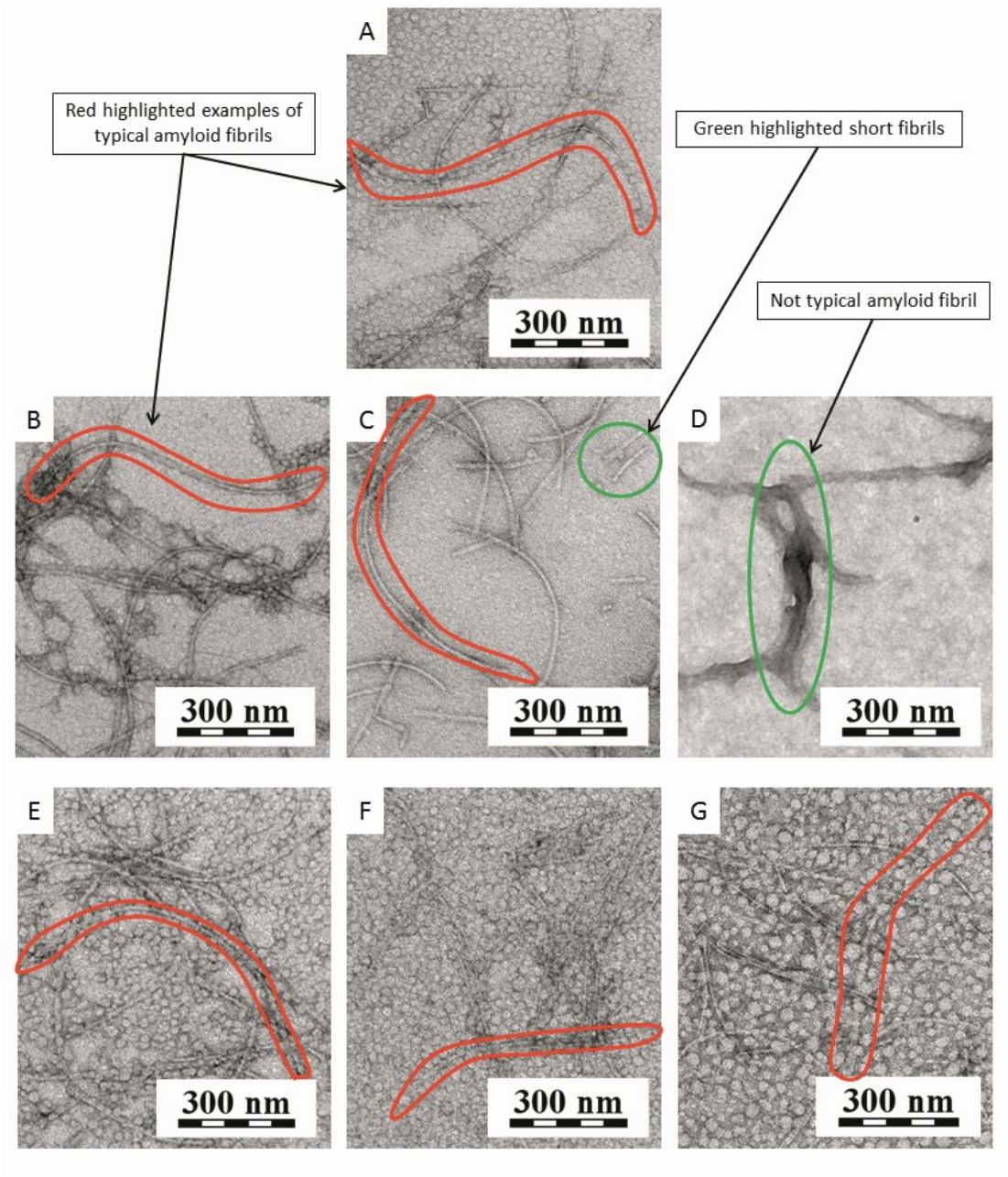

Figure 15. TEM micrographs of experiments with SWNT and C_{60} after 27.5 h incubation: (A) fibrils of HEWL (control) any nanospecies; (B) fibrils of HEWL with 16 µg/mL SWNT; (C) fibrils and shorter fibrils of HEWL with 80 µg/mL SWNT; (D) thick fibrils of HEWL with 250 µg/mL SWNTs; (E) only long typically fibrils of HEWL with 16 µg/mL C_{60}, (F) 80 µg/mL C_{60} and (G) 250 µg/mL C_{60}.

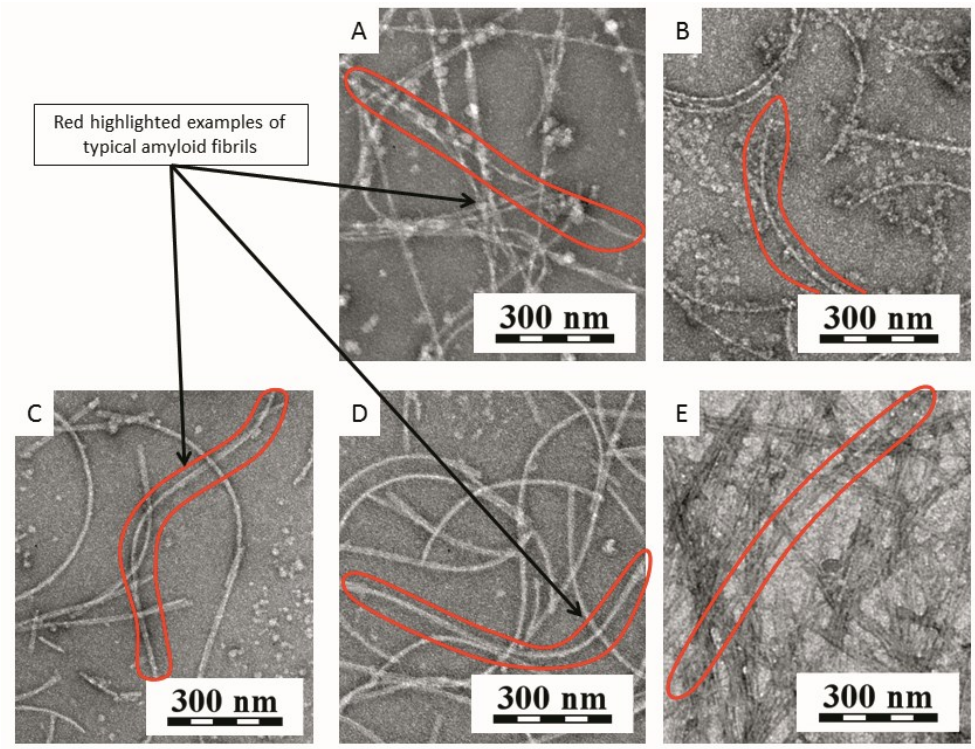

Figure 16. TEM micrographs of experiments with NDs after 23 h incubation: (A) fibrils of HEWL (control); (B) fibrils of HEWL with 16 µg/mL NDs; (C) fibrils of HEWL with 80 µg/mL NDs; (D) fibrils of HEWL with 250 µg/mL NDs; (E) many fibrils of HEWL with 1 mg/mL NDs.

To compare the C_{60} and SWNT experiments and the ND experiments, a graph in Figure 17 was plotted that combines two graphs (Figure 14A and B). The control was taken at a certain time as 100 %, and individual values for C_{60}, SWNT and NDs were calculated according to the control at this particular time. A peak can be observed for all concentrations of NDs (the concentration 1 mg/mL was not plotted on the graph, as it substantially exceeds all the others). The reason for the occurrence of this peak was probably due to the fact that NDs acted as nuclei and amyloid fibrils were immediately formed in their presence, while amyloid fibrils in the control were formed more slowly. The decrease of ND values relative to the control was likely due to the immediate formation of a large number of fibrils in ND presence and a reduction of concentration of free protein to form additional new amyloid fibrils. The graph in Figure 17 supports the results since the highest concentration of C_{60}

accelerated the process of amyloid fibril formation, while the two lower concentrations of C_{60} (16 µg/mL and 80 µg/mL) slowed it down. In case of SWNT, all curves show a decrease. Additionally, it was mentioned that the growth of the fibrils can be terminated on the surface of the SWNT. Based on the obtained results from the comparative graph (Figure 17), it is possible to arrange CNPs from the most to the least amyloidogenic in the following order: NDs > control > C_{60} > SWNT.

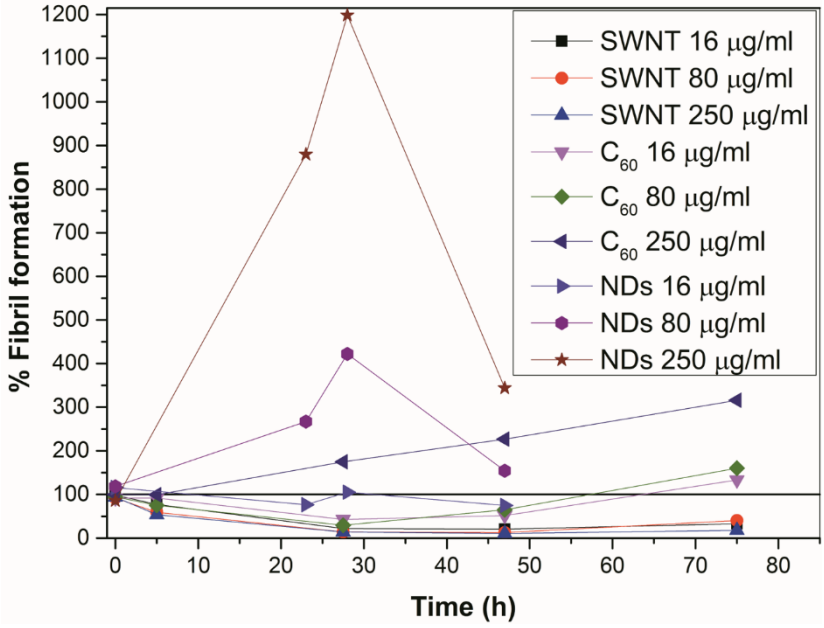

Figure 17. A comparative graph of different concentrations of CNPs at different times.

The last tested CNPs were CDs. As mentioned above, due to CD fluorescence, NR was used instead of ThT for rapid detection of the growth of amyloid fibrils. The results from measuring NR fluorescence are shown in Figure 18. The smallest concentration of CDs (16 µg/mL) did not have any effect on the process of amyloid fibril formation. On the other hand, three other concentrations of CDs (80, 250 and 1000 µg/mL) decelerated the process. This was confirmed by TEM micrographs (see Figure 19). The control reveals long amyloid fibrils (Figure 19A), that are also observed for CDs 16 µg/mL (Figure 19B). However, TEM micrographs of CDs at 80 µg/mL also show shorter fibrils next to long fibrils (Figure 19C).

As the concentration of CD increases, so does the concentration of shorter fibrils (Figure 19D, CDs 250 µg/mL). The highest tested concentration of CDs inhibited the process of amyloid fibril formation. No increase in NR fluorescence was observed for this concentration (Figure 18) and TEM shows no fibrillar morphology (Figure 19E).

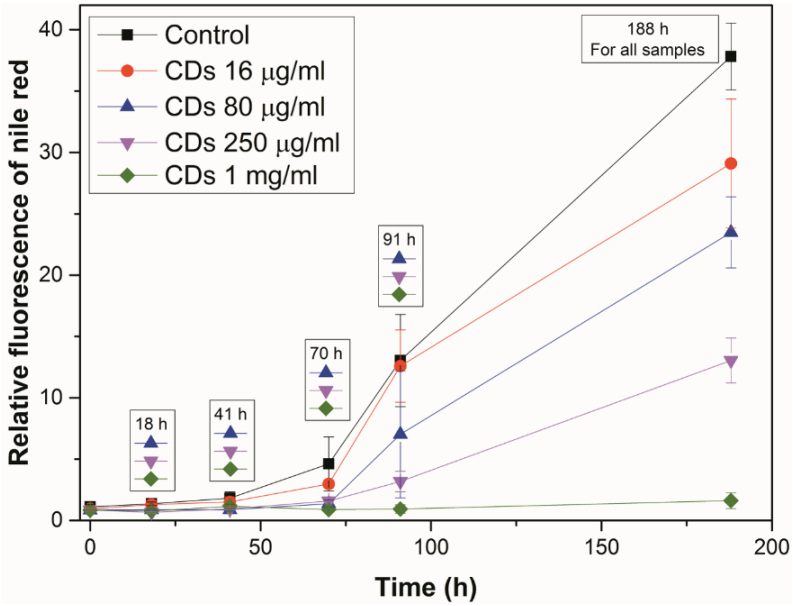

Figure 18. A graph of the relative fluorescence of NR in experiments with CDs. The legend above the results from the same time represents a statistically significant difference ($\alpha<0.05$) when compared to the control at the same time.

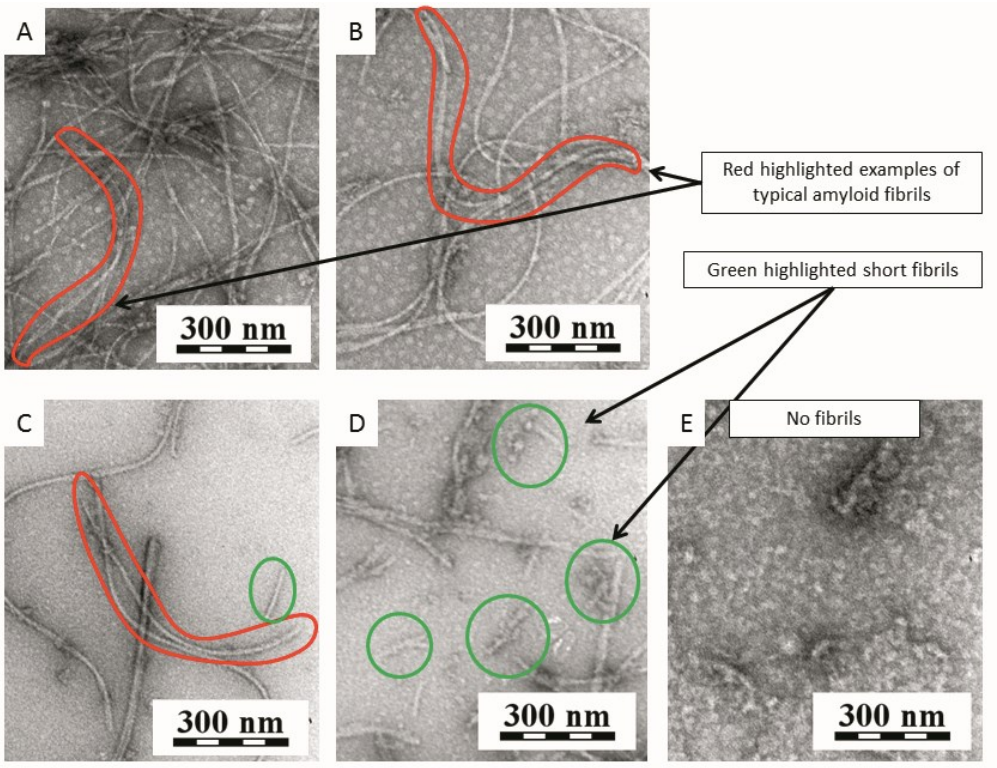

Figure 19. TEM micrographs of experiments with CDs after 25 h incubation: (A) fibrils of HEWL (control); (B) fibrils of HEWL with 16 µg/mL CDs; (C) fibrils and shorter fibrils of HEWL with 80 µg/mL CDs; (D) shorter fibrils of HEWL with 250 µg/mL CDs. (E) no fibrils of HEWL with 1 mg/mL CDs.

At the end of this part, we would like to briefly summarize what is likely to happen to HEWL in the presence of CNPs. Generally, SWNTs have a hydrophobic surface and one side of the β-sheet is also hydrophobic. It is also necessary to emphasize that SWNTs contain sp^2-hybridized carbon, which means that π-π interactions probably play a key role in the process of inhibition. Theories found in the literature are not far from our achieved results. Ghule *et al.*[79] used a different model for testing (human acidic fibroblast growth factor (hFGF-1) and they used MWNT instead of SWNT. However, the effect of SWNT could be similar. Ghule *et al.* proposed a possible mechanism of the effect of MWNTs on the process of amyloid fibril formation. The inhibition of the process might be due to the protein either adsorbing onto the surface of MWNTs or its encapsulation by MWNT[79]. In the case of

SWNTs, adsorption of HEWL on their surface is likely, because SWNTs are smaller than MWNTs, moreover, they have rather closed ends. The mechanism of SWNT inhibition is shown in Figure 20.

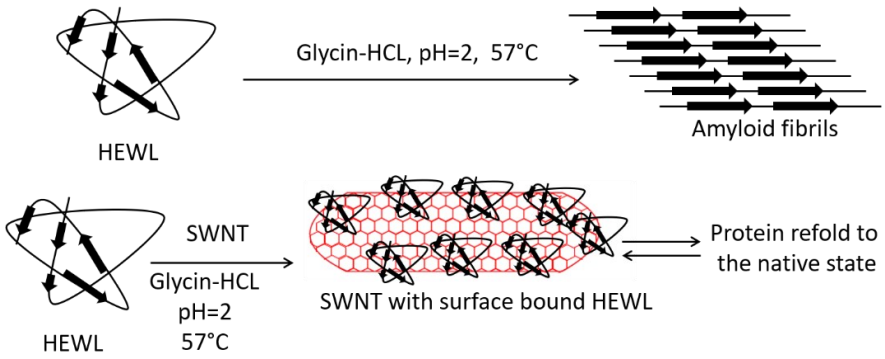

Figure 20. Possible mechanism of SWNT inhibition.

There are molecular dynamics (MD) simulations that were performed by Fu *et al.* [80] and Li *et al.* [81] Fu *et al*. utilized MD simulations to investigate the interactions of $A\beta_{25-35}$ peptide with SWNT. They suggested that the adsorption of $A\beta_{25-35}$ peptides on SWNTs can lead to $A\beta_{25-35}$ opened or closed β-barrels (Figure 21) wrapping SWNT. They also suggested a possible mechanism of interaction between SWNT and the peptide. The main interactions between SWNT and Aβ peptides are hydrophobic, which leads to the formation of β-barrels simultaneously with the dehydration of the SWNT–peptide interface; additionally, intersheet hydrogen bonds are formed[80]. Li *et al.* continued with the determination of SWNT-$A\beta_{16-22}$ interactions by MD simulations. They proposed that hydrophobic, as well as π–π interactions, between $A\beta_{16-22}$ and SWNT may destabilize the β-sheet structure and induce the formation of disordered coil aggregates, which could prolong the lag phase and even reverse the process of amyloid fibril formation[81]. In case of C_{60}, π-π and hydrophobic interactions also played a key role in the effect on the process of amyloid fibril formation. Since inhibition was not

achieved, as in the case of SWNT, the shape of nanospecies and surface curvature may also be important for inhibition.

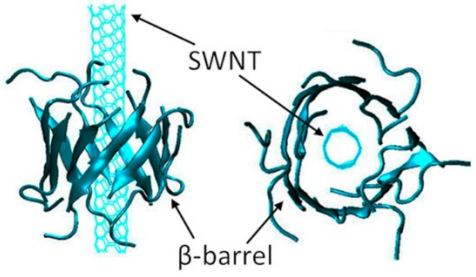

Figure 21. A β-barrel of an $A\beta_{25-35}$-wrapped SWNT[80].

On the other hand, sp^3-hybridized carbon and surface groups which have a positive charge in case of NDs were not suitable for the inhibition of the process of amyloid fibril formation. NDs served as nuclei for the beginning of the process. It was shown that the lag phase was shortened and, subsequently, a rapid creation of fibrils occurred. These results may show the potential hazards of NDs, but on the other hand, NDs may not be that harmful, because oligomers assembled over the course of amyloid formation are more toxic than mature fibrils[38]. However, tailored surface modifications may change the effects of NDs on amyloid formation.

The last tested CNPs, CDs, significantly slowed down and even inhibited (for the concentration of 1 mg/mL) the process of amyloid fibril formation. The π-π and electrostatic interactions probably played the most important role in the effect on the process. From the obtained results, the tested CNPs can be ranked from the most to the least amyloidogenic in the following order NDs > control > C60 > CDs > SWNT.

4.2. Polysaccharides, glycogen modifications and amyloid fibril formation

Glycosaminoglycans (GAGs) as natural polysaccharides have been shown to have an important role in the process of amyloid fibril formation[17]. It was shown, that GAGs, as polyanions, play the main role in catalyzing protein aggregation and stabilizing amyloid fibrils[17]. Although GAGs have been shown to act as promoters, they have the ability to scavenge toxic oligomer forms of amyloid fibrils, thereby reducing toxicity[36] for cells. There are some studies that deal with the effect of GAGs on the process of amyloid fibril formation[35,82–84]. It the past, investigations were reported of the effect of other polysaccharides, such as chitosan[85], glucan (from *Lonicera japonica Thunb.*)[86].

We decided to determine the influence of polysaccharides (glycogen (GG), phytoglycogen (PG) and mannan (MAN)) and several glycogen modifications on the process of amyloid fibril formation. GG is known to be a major storage form of D-glucose in humans and animals, and typical GG concentrations in tissues are: liver, approximately 6-8% by weight[87,88]; muscles, approximately 1-2% by weight[87,88]; brain, approximately 0.1% by weight[89]. In addition, due to the high GG contents in the tissues, high concentrations of glycogen were also tested for amyloidogenicity. PG as a plant analog of GG was chosen for its larger molecular size than GG. The comparison of GG and PG demonstrated the effect of molecule size. MAN is a major soluble polysaccharide constituent of fungal and yeast cell walls, which may be associated to the possible induction of amyloidoses by mycosis[90–93].

As was previously mentioned hydrophobic and electrostatic interactions[32,94] have an important role in amyloid fibril formation, but the key role is played by π–π

interactions[28].Therefore, benzoyl, phenylacetyl or cinnamoyl groups were introduced into the GG structure to compare their effects.

It is also important to mention that minor changes (elimination of the stirrers and using an incubator with shaking) were made to the HEWL model system before this part. As a result, the growth of amyloid fibrils was gradual and visible by both THT fluorescence and TEM. In addition, there was an effort to fit the data according to equation (1). The time $t_{0.5}$ was obtained from the given fit and $t_{lag\ time}$ was calculated according to equation (2). In addition to HEWL, the $A\beta_{1\text{-}42}$ model system was used.

4.2.1. Syntheses of GG modifications

GG was alkylated via a reaction of its alkoxide with benzoyl, phenylacetyl or cinnamoyl chloride to produce the desired modified glycogen (Figure 22). We determined three different aromatic acyls (benzoyl, phenylacetyl, cinnamoyl) in different degree of modifications. The degree of functionalization (number of benzoyl, phenylacetyl or cinnamoyl groups per D-glucose unit) was calculated from the ^{1}H-NMR spectrum and values are included in Table 4.

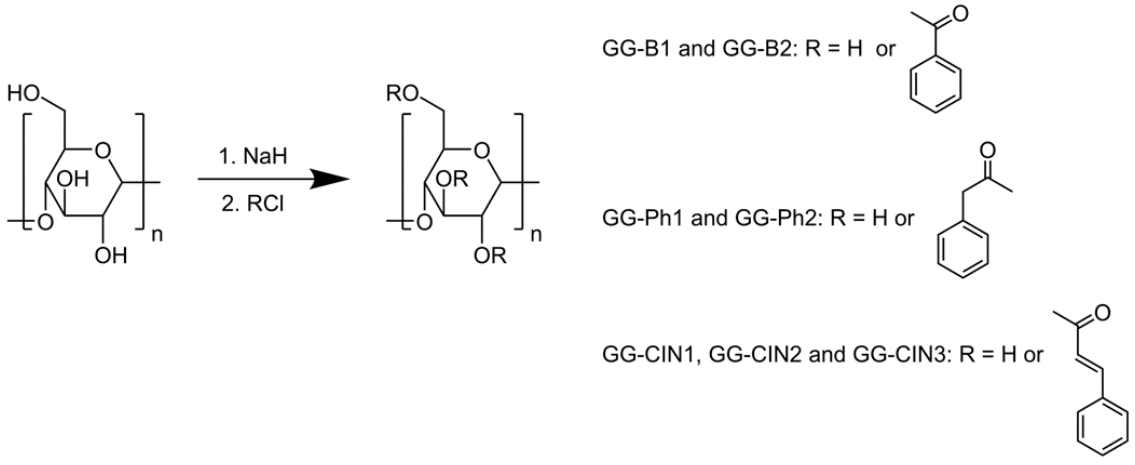

Figure 22. Scheme of syntheses for GG modifications

4.2.2. Characterization of polymers

For the brief characterizations, refractive indexes (dn/dc) were measured, that were used to determine M_w with asymmetric flow field-flow fractionation (AFFFF). The Berry method was used to determine M_w[95]. DLS was also performed to find out R_h. Table 4 summarizes the individual properties of polymers. GG-CIN3 showed two peaks in the distribution of R_h, but the peak for bigger particles contributed a very small proportion to the total molecular weight (approximately 2.8 vol. %). In general, there were rather decreases in M_w of GG modifications, which is consistent with decreases in R_h values.

Table 4. Refractive indexes (dn/dc), molecular weight (M_w) and hydrodynamic radius (R_h) for polysaccharides and GG modifications.

Groups	***Amount of mol. %[a]***	***Name***	***dn/dc***	***M_w (g/mol)***	***R_h(nm)***
		MAN	0.1355±0.0039	5.5×10^4	5.9±1.5
		PG	0.1471±0.0002	27.1×10^6	45.1±19.9
		GG	0.1483±0.0017	5.70×10^6	23.5±8.1
Benzoyl	0.5	GG-B1	0.1380±0.0004	3.80×10^6	20.9±8.3
	1.5	GG-B2	0.1593±0.0007	2.40×10^6	21.7±10.6
Phenylacetyl	1.6	GG-Ph1	0.1613±0.0009	2.50×10^6	19.5±7.9
	2.4	GG-Ph2	0.1490±0.0003	4.00×10^6	20.7±9.7
Cinnamoyl	0.6	GG-CIN1	0.1536±0.0003	4.80×10^6	22.9±10.0
	1.3	GG-CIN2	0.1505±0.0019	6.10×10^6	30.4±10.0
	2.6	GG-CIN3	0.1426±0.0001	7.5×10^6	
				M_{w1} (4.5×10^6)	R_{h1} 20.0±7.1 (97.2 vol %)
				M_{w2} (1.1×10^8)	R_{h2} 143.8.0±63.1 (2.8 vol. %)

[a]determined by ^{1}H-NMR

4.2.3. Amyloid fibril formation of HEWL in the presence of polysaccharides

Figure 23 shows the times ($t_{0.5}$ and $t_{lag\ time}$) for the tested concentrations of polysaccharides. Figure 25 shows the graph of ThT fluorescence with the fit of data for MAN. It was shown, that MAN did not have a strong effect on the process of amyloid fibrils

formation. The main effect of MAN was probably in the growth phase, because the fit of MAN data exhibited a significant shortening of $t_{0.5}$ for 250 µg/mL and 500 µg/mL. All TEM micrographs of MAN samples indicated similar fibril morphology as that of the control. Example of TEM micrographs after 48 h are shown in Figure 24.

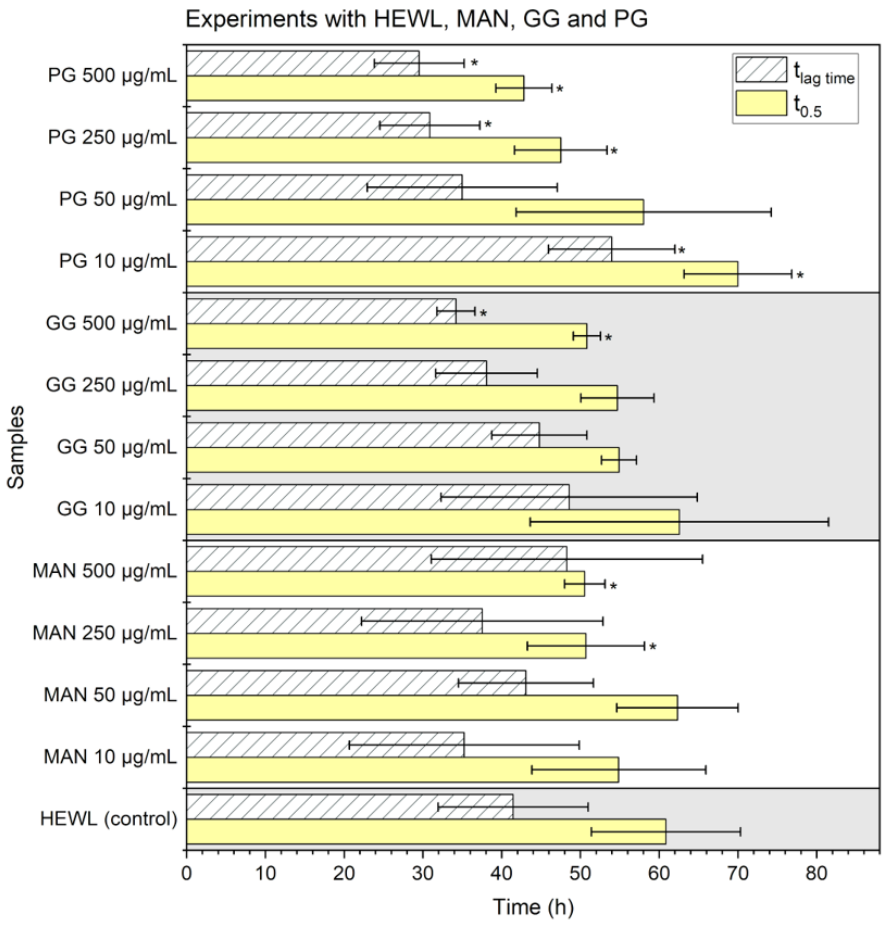

Figure 23. A graph of lag times ($t_{lag\ time}$) and times ($t_{0.5}$) at 50% maximal fluorescence for experiments with HEWL, MAN, GG and PG, according to the data fitted by equation (1) and calculated by equation (2). The asterisk (*) means a statistically significant difference ($\alpha<0.05$) when compared to the control.

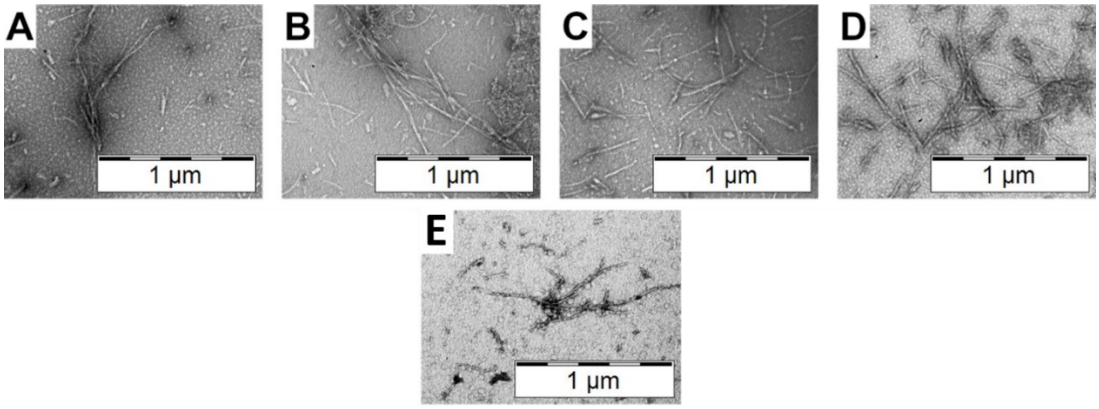

Figure 24. TEM micrographs after 48 h incubation: shorter and longer fibrils for samples containing (A) 10 µg/mL, (B) 50 µg/mL, (C) 250 µg/mL, (D) 500 µg/mL MAN and (E) only HEWL (control).

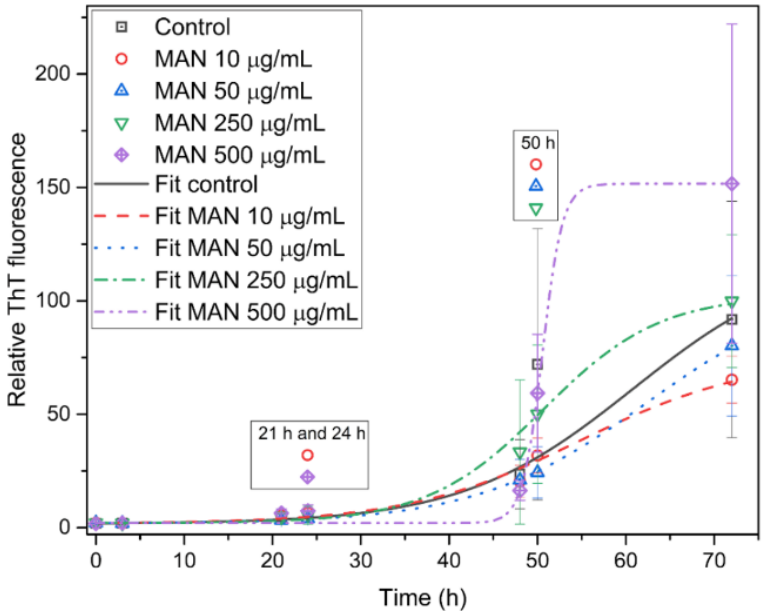

Figure 25. A graph of relative ThT fluorescence with the fit of data for experiments with MAN. The legend above the results from the same time represents a statistically significant difference ($\alpha<0.05$) when compared to the control at this time.

GG and PG have similar structures and effect on the process of amyloid fibril formation. Their influence was dependent on their concentration. The results of ThT fluorescence and an example of TEM micrographs after a 48 h incubation are shown in Figure 26. The fit of ThT fluorescence with 10 µg/mL PG reveals a prolonged lag time, thereby shifting $t_{0.5}$ to higher times (Figure 23). However, a prolonging of the lag phase was not confirmed on the TEM micrographs, because no difference was observed in TEM

micrographs of 10 μg/mL PG and in the control. The higher concentrations of GG (500 μg/mL) and PG (250 μg/mL and 500 μg/mL) accelerated the process of amyloid fibril formation. There was a significantly shortened lag phase (Figure 23). The acceleration of these samples was supported by TEM micrographs after a 48h incubation (Figure 26E-G). All mentioned micrographs reveal mature amyloid fibrils, while the TEM micrograph of the control indicated relatively short fibrils (Figure 26C). Other concentrations did not show any effect on the process of amyloid fibril formation. It is necessary to mention that for the sample with 250 μg/mL GG, there was no statistical difference for the lag time, but the TEM micrograph indicated long fibrils (Figure 26D). Based on the results, a molecule with a hyperbranched polysaccharide surface was probably what promoted amyloid fibril formation. Additionally, GG and PG were compared to evaluate the effect of molecular size on protein-polysaccharide interactions and it has been shown that a system with a larger dimension (PG) speeded up more the process of amyloid fibril formation.

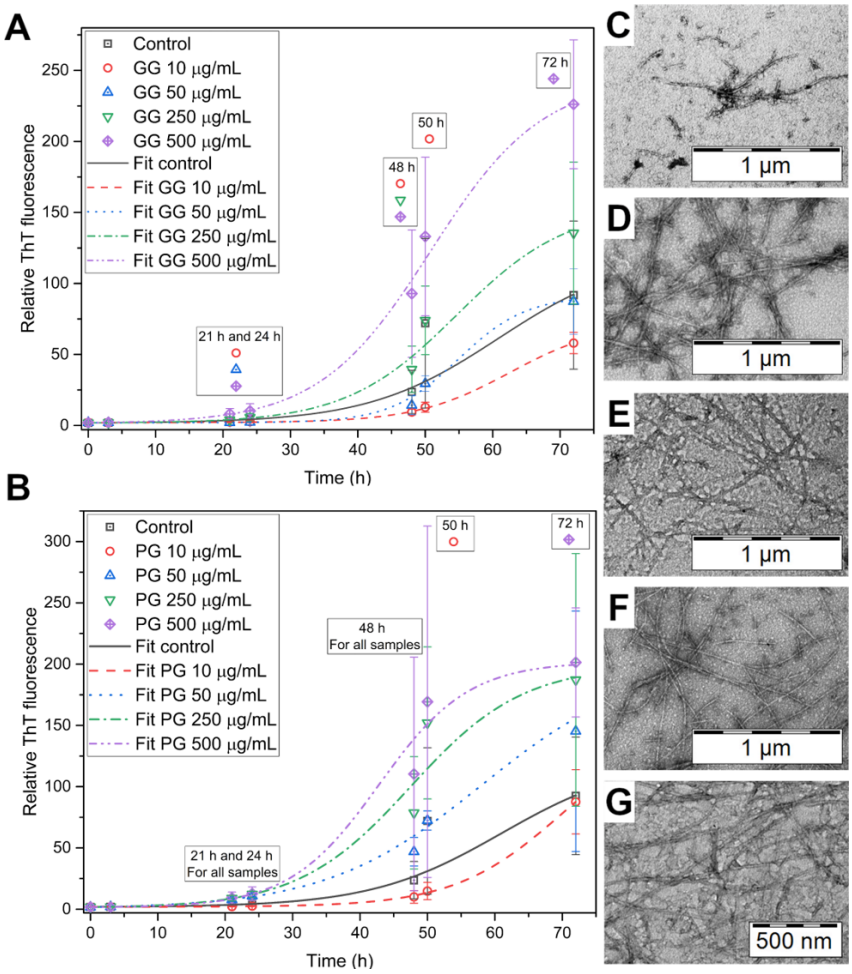

Figure 26. Results of polysaccharides amyloid fibril formation experiments. Graphs of relative ThT fluorescence with the fit of data. The legend above the results from the same time point represents a statistically significant difference ($\alpha<0.05$) when compared to the control at this time. (A) Control (only HEWL) and different concentrations of GG, (B) HEWL and different concentrations of PG. TEM micrographs after 48 h of incubation: (C) shorter fibrils of HEWL; long, mature fibrils for samples containing (D) 250 μg/mL and (E) 500 μg/mL GG and (F) 250 μg/mL and (G) 500 μg/mL PG.

It was decided, that in the case of GG, a high but physiologically relevant concentration would also be tested. The reason was that GG serves as a major storage unit of D-glucose in humans and animals (mainly in the liver and muscles[87,88]). Interesting results were obtained in this experiment, as shown in Figure 27. The acceleration was observed for all concentrations. The highest concentration of GG (25 mg/mL) showed an extremely accelerated process of amyloid fibril formation, which was confirmed by a TEM micrograph

after a 4 h incubation. The control did not show any fibrils, while GG 25 mg/mL revealed fibrils (Figure 27E). In case of 10 mg/mL GG and 5 mg/mL GG, we also observed a high acceleration, because both samples showed long amyloid fibrils in the TEM micrographs after a 24 h incubation (Figure 27I and J), while the control revealed only shorter fibrils (Figure 27F). The acceleration was also observed for the last two concentrations 0.5 mg/mL GG and 1 mg/mL GG. Both concentrations showed long fibrils compared to shorter fibrils of the control (Figure 27L-M).

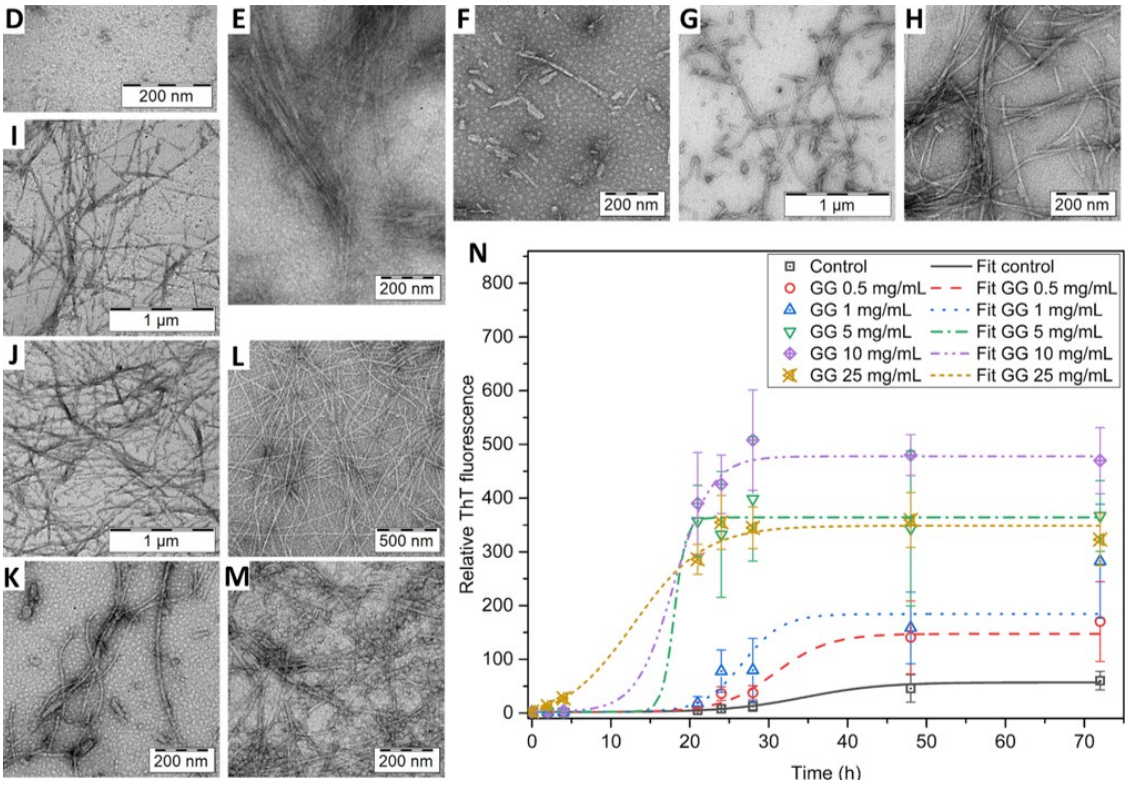

Figure 27. (D-N) Results of the experiments with high concentrations of GG. TEM micrographs after 4 h: (D) any fibrils in the control (only HEWL); (E) fibrils formed with 25 mg/mL GG. TEM micrographs after 24 h: (F) control; (G) 0.5 mg/mL GG; (H) 1 mg/mL GG; (I) 5 mg/mL GG and (J) and 10 mg/mL GG. TEM micrographs after 48 h: (K) control, (L) 0.5 mg/mL GG and (M) 1 mg/mL GG. A worse contrast was observed for uranyl acetate staining of amyloid fibrils and polysaccharides at high concentrations. (N) A graph of relative ThT fluorescence with fitted data for HEWL samples without (control) and with high concentrations of GG.

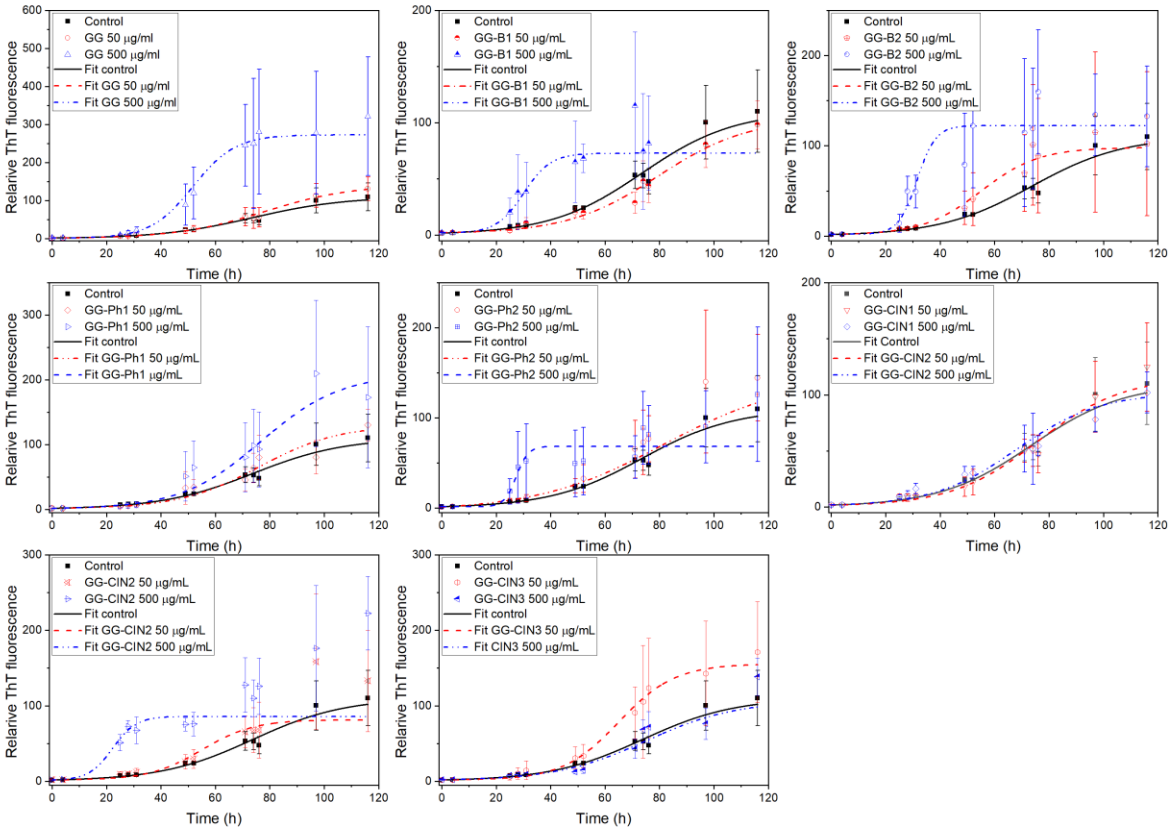

Figure 28. Graphs of ThT fluorescence for GG and all GG modifications with data fits

The results for the other tested groups (GG and GG modifications) are shown in Figure 28, Figure 29, Figure 30 and Figure 31. In the case of benzoylated GG, the GG-B1 (0.5 mol. % benzoyl groups per D-glucose unit) and GG-B2 (1.5 mol. % benzoyl groups per D-glucose unit), the influence on the process was not very pronounced. For higher concentrations (500 μg/mL) of GG-B1 and GG-B2, we observed a shortening of the lag phase. TEM micrograph of GG-B1 after 28 h did not show a big difference in the morphology to the control (Figure 29A and E). A change in morphology was revealed for GG-B2, where we observed clumped short fibrils (Figure 29G). This could be caused by the possible interaction of this GG modification with growing fibrils, which may retard the growth of fibrils.

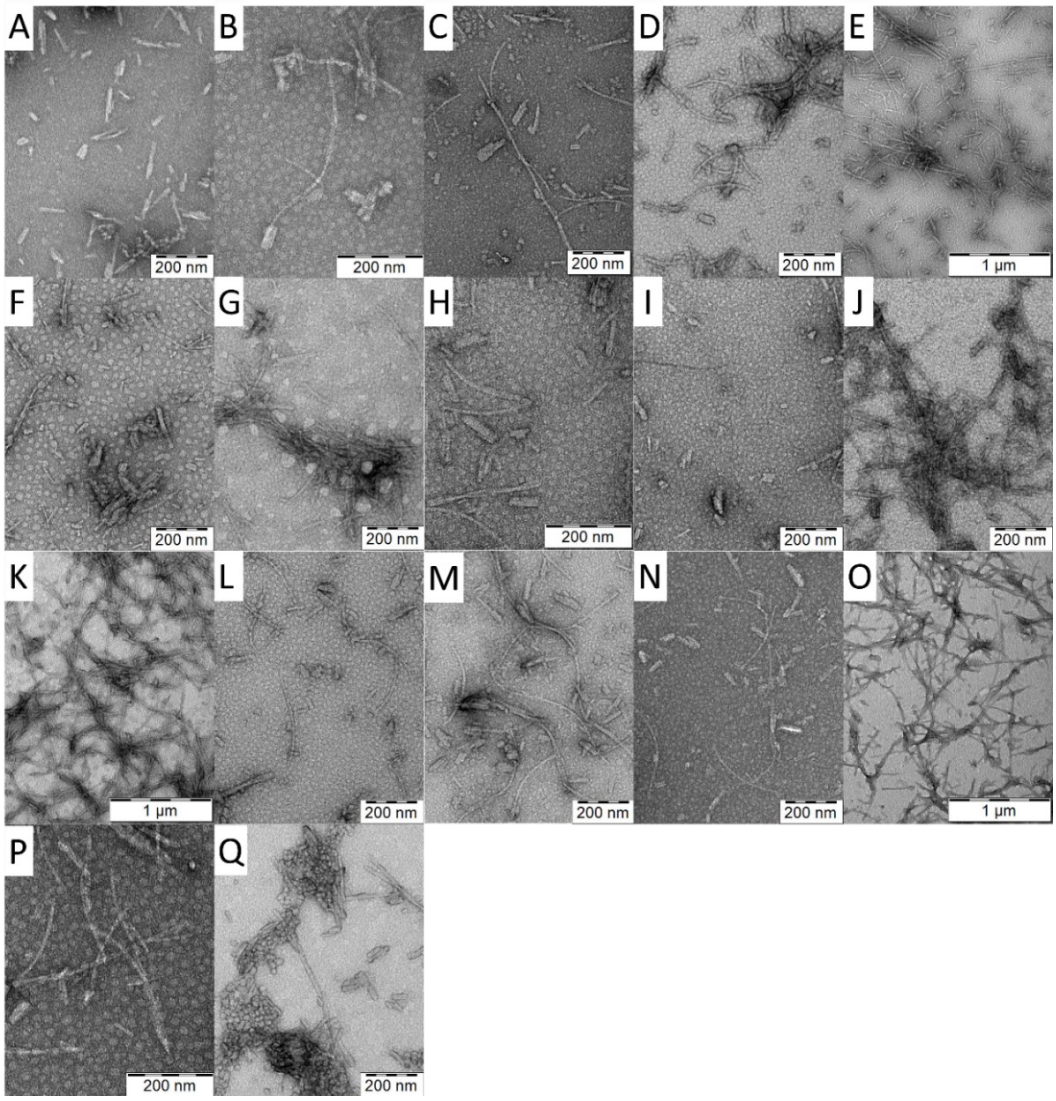

Figure 29. TEM micrographs after 28h incubation: (A) control (only HEWL); (B) 50 µg/mL GG; (C) 500 µg/mL GG; (D) 50 µg/mL GG-B1; (E) 500 µg/mL GG-B1; (F) 50 µg/mL GG-B2; (G) 500 µg/mL GG-B2; (H) 50 µg/mL GG-Ph1; (I) 500 µg/mL GG-Ph1; (J) 50 µg/mL GG-Ph2; (K) 500 µg/mL GG-Ph2; (L) 50 µg/mL GG-CIN1; (M) 500 µg/mL GG-CIN1; (N) 50 µg/mL GG-CIN2; (O) 500 µg/mL GG-CIN2; (P) 50 µg/mL GG-CIN3; (Q) 500 µg/mL GG-CIN3

If we take a closer look at the effect of phenylacetylated GG (GG-Ph1 (1.6 mol. % of phenylacetyl groups per D-glucose unit) and GG-Ph2 (2.4 mol. % of phenylacetyl groups per D-glucose unit)), we find that their behavior is different. GG-Ph1 prolonged the lag phase for both concentrations. Their TEM micrographs after a 28h incubation (Figure 29H and I) revealed similar morphology to the control (shorter fibrils and some “nuclei”), but TEM

micrographs after a 76 h incubation for a concentration of 50 µg/mL show a hint of clumped short fibrils (Figure 30H). In the case of the concentration of 500 µg/mL, we can see only clumped short fibrils (Figure 30I), while the control reveals variously folded long mature fibrils (Figure 30A). It is probably a similar effect to GG-B2. On the other hand, the second modification GG-Ph2 significantly shortened the lag phase for both concentrations, which was also observed in TEM micrographs after a 28h incubation, because we can see a long mature fibril (Figure 29J and K).

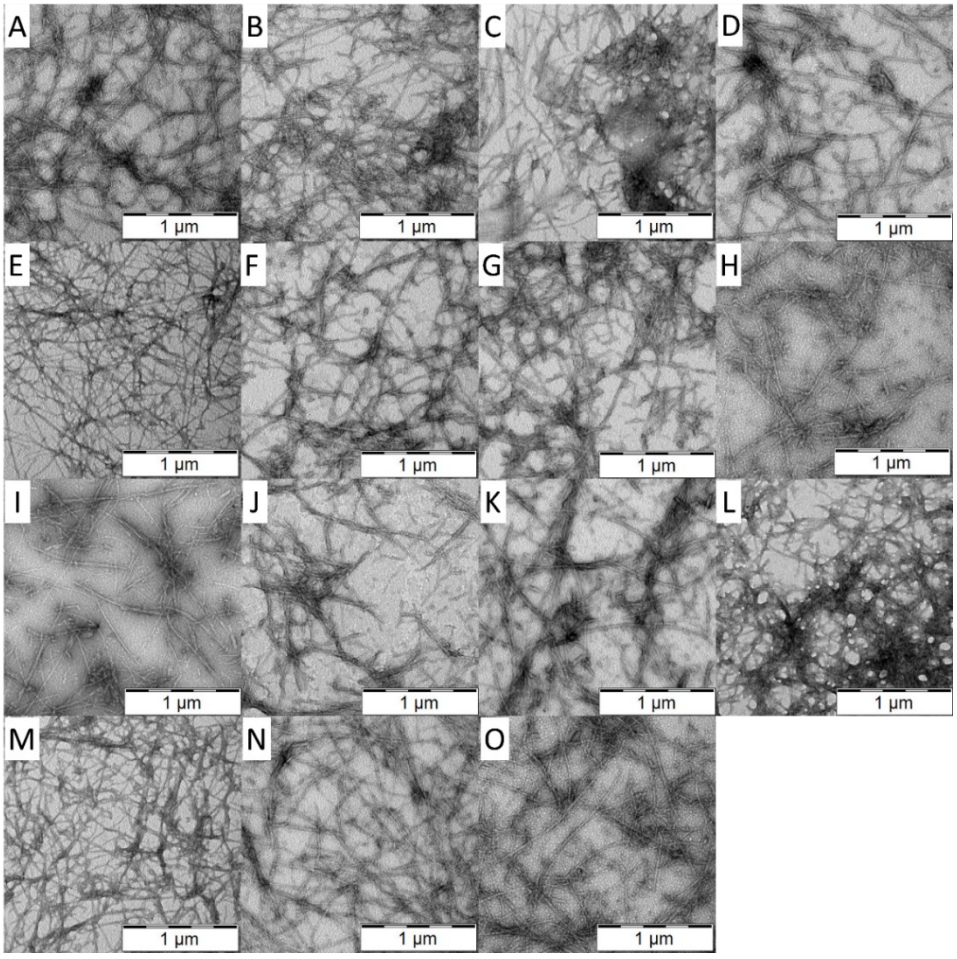

Figure 30. TEM micrographs after 76h incubation: (A) control (only HEWL); (B) 50 µg/mL GG; (C) 500 µg/mL GG; (D) 50 µg/mL GG-B1; (E) 500 µg/mL GG-B1; (F) 50 µg/mL GG-B2; (G) 500 µg/mL GG-B2; (H) 50 µg/mL GG-Ph1; (I) 500 µg/mL GG-Ph1; (J) 50 µg/mL GG-Ph2; (K) 50 µg/mL GG-CIN1; (L) 500 µg/mL GG-CIN1; (M) 50 µg/mL GG-CIN2; (N) 50 µg/mL GG-CIN3; (O) 500 µg/mL GG-CIN3

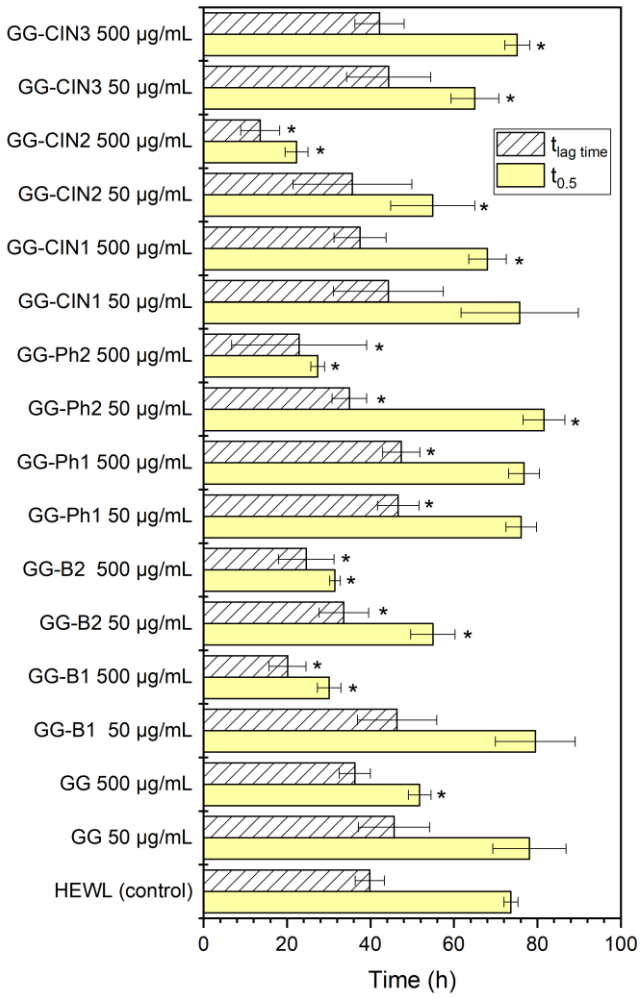

Figure 31. A graph of $t_{lag\ time}$ and $t_{0.5}$ for experiments with HEWL, GG and GG modifications, according to the data fitted by equation (1). The star (*) represents a statistically significant difference ($\alpha<0.05$) when compared to the control (only HEWL).

The last tested samples were three cinnamoyl-modified GG (GG-CIN1 (0.6 mol. % cinnamoyl groups per D-glucose unit), GG-CIN2 (1.3 mol. % cinnamoyl groups per D-glucose unit) and GG-CIN3 (2.6 mol. % cinnamoyl groups per D-glucose unit). GG-CIN1 showed similar behavior to GG. However, GG-CIN2 significantly shortened the lag phase for the concentration of 500 µg/mL. Long mature amyloid fibers occurred after one day incubation (Figure 29O). On the other hand, the most densely cinnamoylated GG-CIN3 did not appear to influence the lag phase, but its effect was probably on the growth phase. The

time $t_{0.5}$ was prolonged for both concentrations of GG-CIN3, which was probably due to the interaction of GG-CIN3 with the growing fibril and it could slightly prolong its growth (see Figure 29Q).

4.2.4. Effect of polysaccharide and modified GG on HEWL

DLS measurements were performed to determine the effect of temperature on polysaccharides and GG modifications without HEWL and in the presence of HEWL (20°C–57°C with increments of 1 °C). DLS was measured for all tested polymers, but we have chosen for display only those where a change was observed. Figure 32 displays the temperature dependence of R_h of various objects identified in the size distributions.

A slightly decreasing R_h was found with increasing temperature for all polymers. The R_h for HEWL was also measured. It was approximately 2 nm, which was consistent with the literature[96]. Graph A in Figure 32 shows a slight increase of R_h in the system with GG and HEWL. The increase of R_h was observed immediately after mixing, which could mean that HEWL interacted with GG. This may suggest the molecular mechanism of the acceleration of fibrillation. An interesting situation was observed in GG-B2 (1.5 % benzoyl groups per D-glucose unit). There is only one peak without the presence of HEWL (red dots, in Figure 32B). In the presence of HEWL, we can see two peaks. In the presence of HEWL, GG-B2 formed other bigger particles (blue triangles, Figure 32B), but R_h of smaller particles is lower than GG-B2 without the presence of HEWL. There can be two explanations: (1) Particles of GG-B2 (above to ~ 20 nm) probably interacted with HEWL and formed bigger particles above 100 nm. (2) Formation of bigger particles could be caused by the presence of HEWL, because the solubility of GG-B2 changes in the presence of another substance (in this case

HEWL). Both explanations may confirm experiments of HEWL fibrillation, that GG-B1 had a weaker effect than GG-B2.

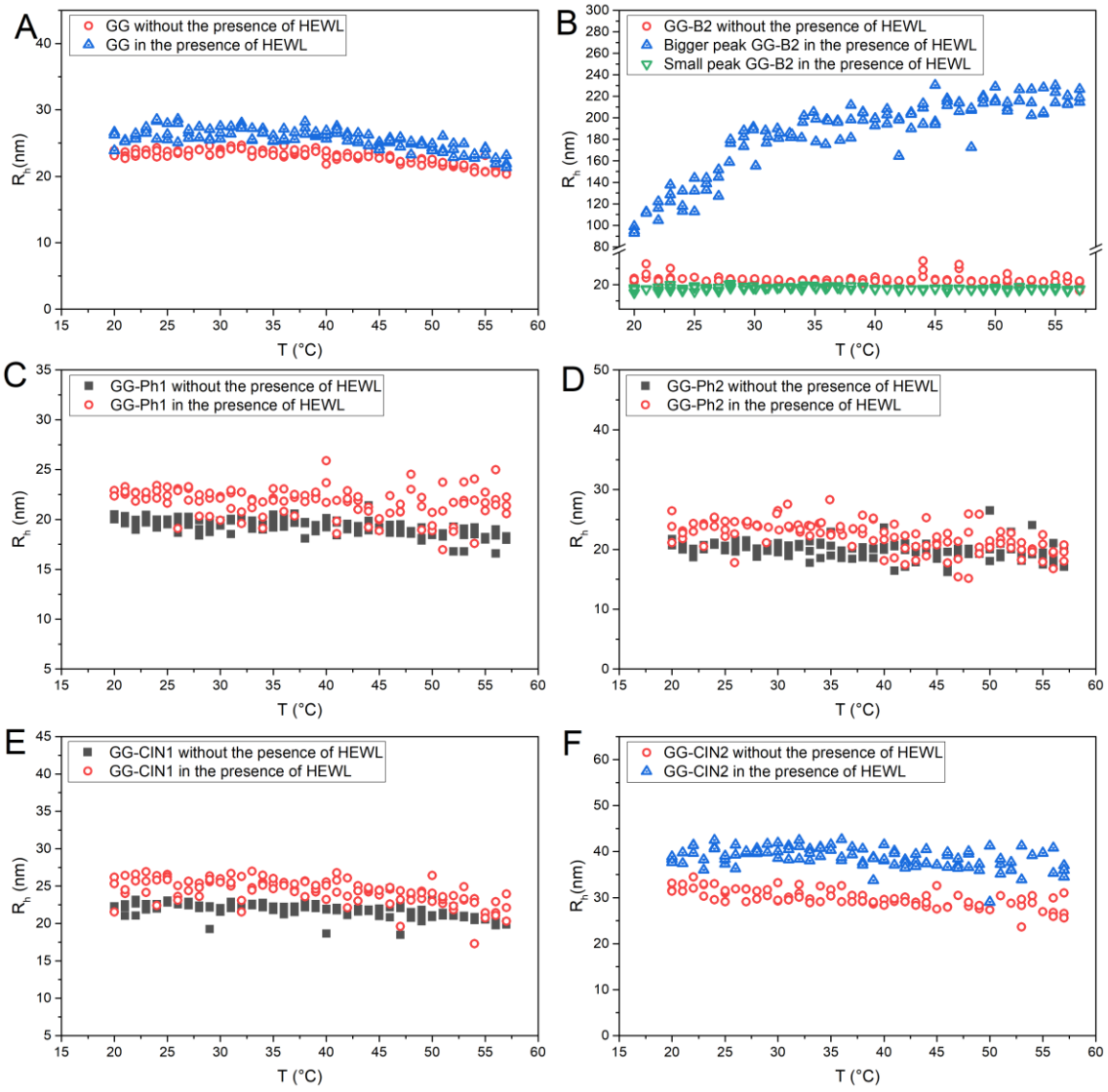

Figure 32. Dependence of hydrodynamic radius R_h on temperature for the solutions of modifications without the presence of HEWL or in the presence of HEWL. (A) GG; (B) GG-B2, (C) BB-Ph1; (D) GG-Ph2; (E) GG-CIN1; (F) GG-CIN2

Two other modifications, GG-Ph1 (1.6 mol.% phenylacetyl groups per D-glucose unit) and GG-Ph2 (2.4 mol.% phenylacetyl groups per D-glucose unit), showed a little increase of R_h in the presence of HEWL. The R_h increase was more noticeable for GG-Ph1 than for GG-Ph2, which could mean only a weak or no interaction between GG-Ph2 and

HEWL. This is consistent with the fluorescence data because their effect on HEWL fibrillation was different. In the case of the last two polymers, GG-CIN1 (0.5 mol. % cinnamoyl groups per D-glucose unit) and GG-CIN2 (1.3 mol. % cinnamoyl groups per D-glucose unit), we found an increase of the R_h polymer in the presence of HEWL. GG-CIN1 did not have such a big increase as GG-CIN2. These data suggest a direct interaction of GG-CIN1 and GG-CIN2 with HEWL, which may cause the shortening of the lag phase in fluorescence experiments.

The final part provides some information about ITC. The ITC measurement was in very good agreement with the data of DLS measurement and fluorescence measurements. ITC measurement of GG confirmed the existence of GG-HEWL complex detected in DLS. In case of GG modifications, we observed the binding of HEWL - the strongest for GG-CIN2, weaker for GG-Ph1 and almost negligible for GG-B2.

4.2.5. Influence of polysaccharides and GG modifications on Aβ$_{1-42}$ fibrillation

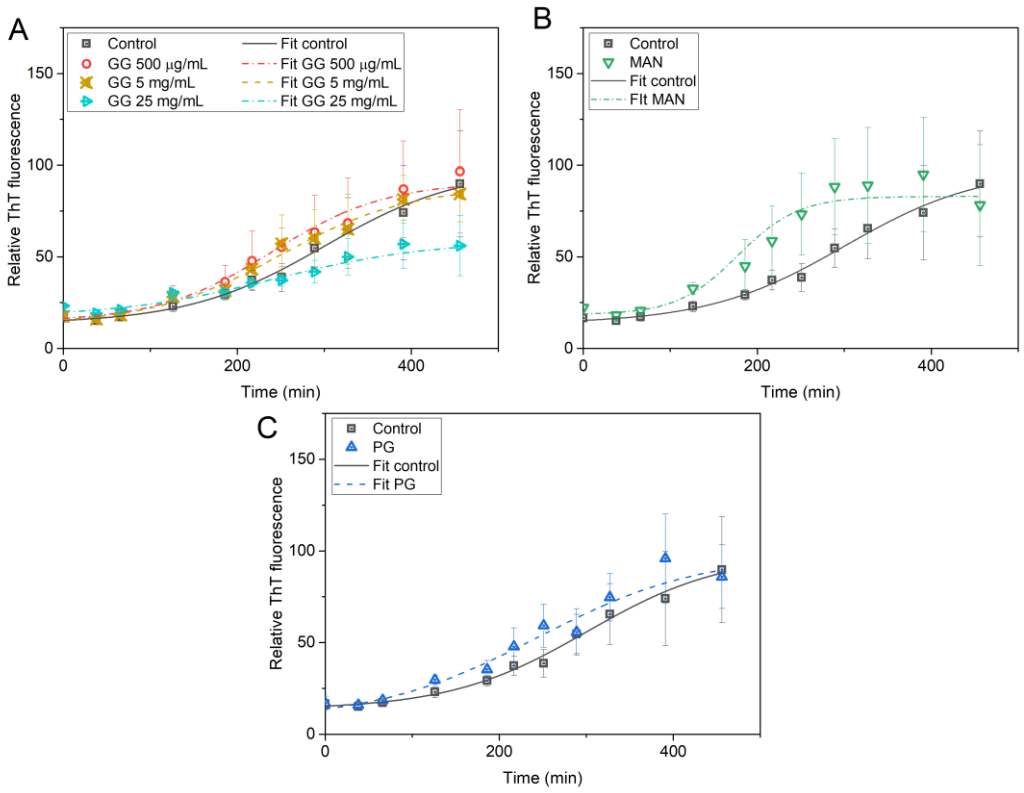

Figure 33. Graphs of relative fluorescence of ThT, where black symbols are control data (Aβ$_{1-42}$ without polysaccharides). (A) experiments for 500 µg/mL, 5 mg/mL and 25 mg/mL GG; (B) experiments for 500 µg/mL MAN; (C) experiments for 500 µg/mL PG

The results obtained for Aβ$_{1-42}$ were in good agreement with data from HEWL fibrillation. The graphs of ThT fluorescence for polysaccharides are shown in Figure 33. Although MAN did not significantly affect the amyloid fibril formation from HEWL, its effect was very drastic in the presence of Aβ$_{1-42}$. It was shown that both PG and GG shortened the lag phase of Aβ$_{1-42}$ fibrillation but only slightly accelerated the growth phase of Aβ$_{1-42}$. The highest concentration of GG (25 mg/ml) dramatically shortened the lag phase, but also prolonged the growth phase, from which we concluded that there is an interaction between Aβ$_{1-42}$ and GG. Because some peptides were blocked, the concentration of Aβ$_{1-42}$ in solution

decreased, which would explain why a concentration of 25 mg/mL GG prolonged the growth phase.

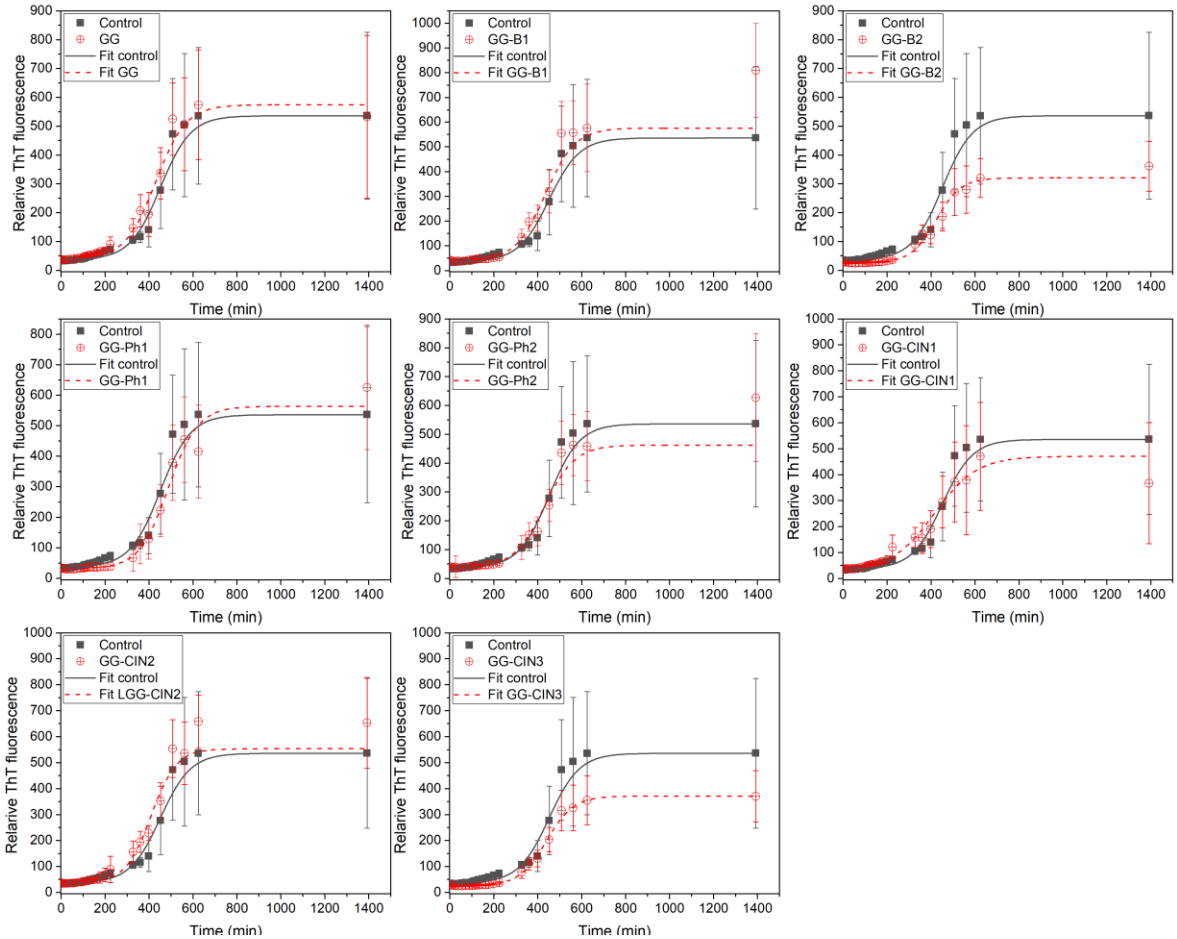

Figure 34. Graphs of relative ThT fluorescence with black symbols represent control data ($A\beta_{1-42}$ without modifications or GG) and fit of measured data.

The results of experiments with GG and GG modifications are shown in Figure 34 and Figure 35. No effect was observed on the lag phase $A\beta_{1-42}$ for GG-B1 (0.5 mol. % benzoyl groups per D-glucose unit) and GG-B2 (0.5 mol. % benzoyl groups per D-glucose unit). Both GG-B1 and GG-B2 slightly accelerated the growth phase. As for the HEWL model, GG-Ph1 (1.6 mol.% phenylacetyl groups per D-glucose unit) also significantly prolonged the lag time, while GG-Ph2 (2.4 mol.% phenylacetyl groups per D-glucose unit) significantly shortened it. The last three cinnamoylated modifications (GG-CIN1 (0.5 mol. %

cinnamoyl groups per D-glucose unit), GG-CIN2 (1.3 mol. % cinnamoyl groups per D-glucose unit) and GG-CIN3 (2.6 mol. % cinnamoyl groups per D-glucose unit) also showed similar results as in the HEWL model. GG-CIN1 and GG-CIN2 shortened the lag phase, while GG-CIN3 did not have an effect on the lag phase. However, GG-CIN3 shortened the growth phase.

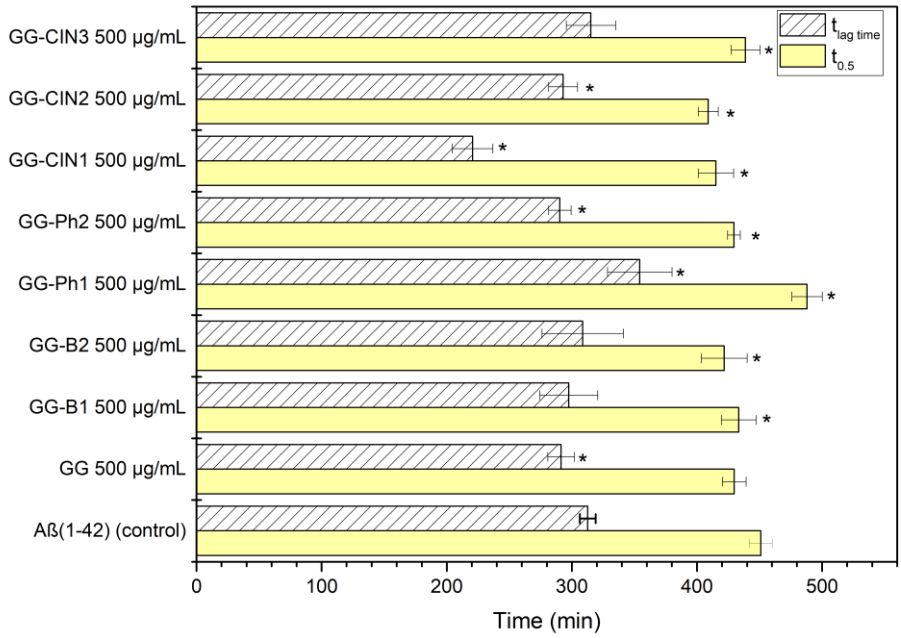

Figure 35. A graph of $t_{lag\ time}$ and $t_{0.5}$ for experiments with $A\beta_{1-42}$, GG and GG modifications, according to the data fitted by equation (1). The star (*) represents a statistically significant difference ($\alpha<0.05$) when compared to the control (only $A\beta_{1-42}$).

5. Conclusion

Testing amyloidogenicity is very complex. Nevertheless, these studies provide useful findings for a wide range of materials. The influence of nanospecies on the process of amyloid fibril formation is dependent on their size, shape and surface. Fibrillation is influenced by the affinity of a protein to nanospecies surface. The π–π, hydrophobic and electrostatic interactions play an important role in the inhibition and acceleration of amyloid fibril formation, and our results confirmed the importance of these interactions.

Based on the obtained results, we have advanced our overall understanding of the influence of CNPs on amyloid fibril formation as follows:

- The study brought an interesting comparison of four different types of CNPs based on various applications. When the amyloidogenicity of all four types of CNPs was compared, the following trend was apparent: NDs > control > C_{60} > CDs > SWNTs.

In the case of polysaccharide (GG, PG and MAN), it was found:

- With increasing concentrations of PG and GG, HEWL fibril formation was promoted, while MAN had a very weak influence on amyloid fibril formation.
- Physiologically relevant concentrations of GG tremendously accelerated HEWL fibril formation, but it was found by DLS and ITC that this effect was most plausibly not due to the crowding effect but caused by direct HEWL and GG interaction.
- The results obtained for HEWL and $A\beta_{1-42}$ were in great agreement.

- MAN did not have a drastic effect on HEWL, but $A\beta_{1-42}$ readily formed fibrils in the presence of MAN. This is relevant for the eventual promoting effect of fungal/yeast parasites on amyloid formation.
- PG and GG shortened the lag phase of $A\beta_{1-42}$ but only slightly accelerated the growth phase of $A\beta_{1-42}$.
- The highest concentration of GG shortened the lag phase of $A\beta_{1-42}$ but prolonged the growth phase because of the direct interaction of GG and $A\beta_{1-42}$.

For the group of modified GGs was determined:

- Slight changes in the polysaccharide surface led to different behaviours (GG vs GG modifications)
- GG-CIN2 (1.3 mol. % cinnamoyl groups per D-glucose unit) and GG-Ph2 (2.4 mol. % phenylacetyl groups per D-glucose unit) had a rapid acceleration effect on the process of amyloid fibril formation
- Modifications with benzoyl groups did not have such a big effect as phenylacetyl groups or cinnamoyl groups.
- The most interesting fact was that GG-Ph1 (1.6 mol. % phenylacetyl groups per D-glucose unit) had a retarding effect compared to all other modifications.

All results indicate the importance of the surface and show how relatively small changes in structure may strongly influence the amyloidogenicity of materials. These points are important particularly in the design of drug delivery systems.

Testing for amyloidogenicity is very difficult because of the work with proteins/peptides. Despite the difficulty, repeatability of experiments can be achieved. In

addition to the mentioned materials, a number of synthetic polymers are planned to be tested, which we assume could have an inhibitory effect. So far, we have tested everything *in vitro*, but it is possible to extend to *in vivo* testing in the future. For *in vivo* testing, there is a simple mouse model, where injection of $AgNO_3$ can be used to experimentally induce secondary systemic amyloidosis (AA-amyloidosis)[97]. Another possible model for *in vivo* is using rotenone which induces the accumulation of α-synuclein in rats[98] and has been used to establish an animal model of Parkinson's disease[99].

6. References

1. Radford, S. E. & Weissman, J. S. Special Issue: The Molecular and Cellular Mechanisms of Amyloidosis. *J. Mol. Biol.* **421**, 139–141 (2012).
2. Sideras, K. & Gertz, M. A. Amyloidosis. *Advances in clinical chemistry* **47**, 1–44 (2009).
3. J. D. Sipe. Overview of Amyloidosis and Amyloid Proteins. *WILEY-VCH Verlag GmbH Co. KGaA, Weinheim* (2005).
4. Benson, M. D. *et al.* Amyloid nomenclature 2018: recommendations by the International Society of Amyloidosis (ISA) nomenclature committee. *Amyloid* **25**, 215–219 (2018).
5. Hazenberg, B. P. C. Amyloidosis. A clinical overview. *Rheum. Dis. Clin. North Am.* **39**, 323–345 (2013).
6. Fowler, D. M. *et al.* Functional amyloid formation within mammalian tissue. *PLoS Biol.* **4**, 0100–0107 (2006).
7. Wei, G. *et al.* Self-assembling peptide and protein amyloids: from structure to tailored function in nanotechnology. *Chem. Soc. Rev.* (2017). doi:10.1039/C6CS00542J
8. Dueholm, M. S. *et al.* Fibrillation of the Major Curli Subunit CsgA under a Wide Range of Conditions Implies a Robust Design of Aggregation. *Biochemistry* **50**, 8281–8290 (2011).
9. Cherny, I. & Gazit, E. Amyloids: Not only pathological agents but also ordered nanomaterials. *Angew. Chemie - Int. Ed.* **47**, 4062–4069 (2008).
10. Benson, M. D. Amyloidosis and Other Protein Deposition Diseases. in *Reference Module in Biomedical Sciences* 1–18 (Elsevier, 2014). doi:10.1016/B978-0-12-801238-3.05551-3
11. Picken, M. M. Modern Approaches to the Treatment of Amyloidosis. *Adv. Anat. Pathol.* **20**, 424–439 (2013).
12. Iannuzzi, C., Maritato, R., Irace, G. & Sirangelo, I. Misfolding and Amyloid Aggregation of Apomyoglobin. *Int. J. Mol. Sci.* **14**, 14287–14300 (2013).
13. Rambaran, R. N. & Serpell, L. C. Amyloid fibrils: abnormal protein assembly. *Prion* **2**, 112–117 (2008).
14. Porat, Y., Abramowitz, A. & Gazit, E. Inhibition of amyloid fibril formation by polyphenols: Structural similarity and aromatic interactions as a common inhibition mechanism. *Chem. Biol. Drug Des.* **67**, 27–37 (2006).
15. Bartolini, M. & Andrisano, V. Strategies for the inhibition of protein aggregation in human diseases. *ChemBioChem* **11**, 1018–1035 (2010).
16. Rochet, J.-C. & Lansbury, P. T. Amyloid fibrillogenesis: themes and variations. *Curr. Opin. Struct. Biol.* **10**, 60–68 (2000).
17. Sideras, K. & Gertz, M. A. Chapter 1 Amyloidosis. in *Advances in clinical chemistry* **47**, 1–44 (2009).
18. Serpell, L. C. *et al.* The protofilament substructure of amyloid fibrils. *J. Mol. Biol.* **300**, 1033–1039 (2000).
19. Lazo, N. D. & Downing, D. T. Amyloid Fibrils May Be Assembled from β-Helical Protofibrils †. *Biochemistry* **37**, 1731–1735 (1998).
20. Sipe, J. D. & Cohen, A. S. Review: History of the Amyloid Fibril. *J. Struct. Biol.* **130**, 88–98 (2000).

21. Merlini, G. & Bellotti, V. Molecular Mechanisms of Amyloidosis. *N. Engl. J. Med.* **349**, 583–596 (2003).
22. Bemporad, F. & Chiti, F. Pathways of Amyloid Formation. in *Amyloid Fibrils and Prefibrillar Aggregates* 151–166 (Wiley-VCH Verlag GmbH & Co. KGaA, 2013). doi:10.1002/9783527654185.ch8
23. Arosio, P., Knowles, T. P. J. & Linse, S. On the lag phase in amyloid fibril formation. *Phys. Chem. Chem. Phys.* **17**, 7606–7618 (2015).
24. Freire, S., De Araujo, M. H., Al-Soufi, W. & Novo, M. Photophysical study of Thioflavin T as fluorescence marker of amyloid fibrils. *Dye. Pigment.* **110**, 97–105 (2014).
25. Nielsen, L. *et al.* Effect of environmental factors on the kinetics of insulin fibril formation: Elucidation of the molecular mechanism. *Biochemistry* **40**, 6036–6046 (2001).
26. Wallin, C. *et al.* Mercury and alzheimer's disease: Hg(II) ions display specific binding to the amyloid-β peptide and hinder its fibrillization. *Biomolecules* **10**, 44 (2020).
27. Chuang, E., Hori, A. M., Hesketh, C. D. & Shorter, J. Amyloid assembly and disassembly. *J. Cell Sci.* **131**, jcs189928 (2018).
28. Gazit, E. Mechanisms of amyloid fibril self-assembly and inhibition. *FEBS J.* **272**, 5971–5978 (2005).
29. Makin, O. S., Atkins, E., Sikorski, P., Johansson, J. & Serpell, L. C. Molecular basis for amyloid fibril formation and stability. *Proc. Natl. Acad. Sci.* **102**, 315–320 (2005).
30. Makin, O. S. & Serpell, L. C. Structures for amyloid fibrils. *FEBS J.* **272**, 5950–5961 (2005).
31. Marshall, K. E., Morris, K. L., Charlton, D. & O'Reilly, N. Hydrophobic, Aromatic, and Electrostatic Interactions Play a Central Role in Amyloid Fibril Formation and Stability - Biochemistry (ACS Publications). *Biochemistry* 2061–2071 (2011).
32. Chiti, F. & Dobson, C. M. Protein Misfolding, Functional Amyloid, and Human Disease. *Annu. Rev. Biochem.* **75**, 333–366 (2006).
33. Chi, E. Y., Krishnan, S., Randolph, T. W. & Carpenter, J. F. No Title. *Pharm. Res.* **20**, 1325–1336 (2003).
34. Hori, Y., Hashimoto, T., Nomoto, H., Hyman, B. T. & Iwatsubo, T. Role of apolipoprotein E in β-amyloidogenesis: Isoform-specific effects on protofibril to fibril conversion of Aβ in vitro and brain Aβ deposition in vivo. *J. Biol. Chem.* **290**, 15163–15174 (2015).
35. Díaz-Nido, J., Wandosell, F. & Avila, J. Glycosaminoglycans and β-amyloid, prion and tau peptides in neurodegenerative diseases. *Peptides* **23**, 1323–1332 (2002).
36. Valle-Delgado, J. J. *et al.* Modulation of Aβ 42 fibrillogenesis by glycosaminoglycan structure. *FASEB J.* **24**, 4250–4261 (2010).
37. Rosú, S. A. *et al.* Learning from Synthetic Models of Extracellular Matrix; Differential Binding of Wild Type and Amyloidogenic Human Apolipoprotein A-I to Hydrogels Formed from Molecules Having Charges Similar to Those Found in Natural GAGs. *Protein J.* **36**, 374–383 (2017).
38. Sengupta, U., Nilson, A. N. & Kayed, R. The Role of Amyloid-β Oligomers in Toxicity, Propagation, and Immunotherapy. *EBioMedicine* **6**, 42–49 (2016).
39. Bhushan, B. *Springer handbook of nanotechnology*. (2007).
40. Khatra, D. S., Harikumar, S. L. & Nirmala, N. Nanoparticles: An Overview. *J. Drug Deliv. Ther.* **3**, 1121–1127 (2013).

41. Murthy, S. K. Nanoparticles in modern medicine: state of the art and future challenges. *Int. J. Nanomedicine* **2**, 129–41 (2007).
42. Ngô, C. & Van de Voorde, M. H. Nanomaterials: Doing More with Less. in *Nanotechnology in a Nutshell* 55–70 (Atlantis Press, 2014). doi:10.2991/978-94-6239-012-6_4
43. Horikoshi, S. & Serpone, N. Introduction to Nanoparticles. in *Microwaves in Nanoparticle Synthesis* (eds. Horikoshi, S. & Serpone, N.) 1–24 (Wiley-VCH Verlag GmbH & Co. KGaA, 2013). doi:10.1002/9783527648122.ch1
44. Gogotsi, I. G. *Nanomaterials handbook*. (CRC/Taylor & Francis, 2006).
45. Savolainen, K. *et al.* Risk assessment of engineered nanomaterials and nanotechnologies—A review. *Toxicology* **269**, 92–104 (2010).
46. Ashby, M. F., Ferreira, P. J. S. G. & Schodek, D. L. *Nanomaterials, nanotechnologies and design : an introduction for engineers and architects*. (Butterworth-Heinemann, 2009).
47. Ramsden, J. *Applied Nanotechnology.* (Elsevier, 2009).
48. Shatkin, J. A. *Nanotechnology: health and environmental risks*. (CRC Press/Taylor & Francis Group, 2008).
49. Handy, R. D. & Shaw, B. J. Toxic effects of nanoparticles and nanomaterials: Implications for public health, risk assessment and the public perception of nanotechnology. *Heal. Risk Soc.* **9**, 125–144 (2007).
50. Tuzar, Z., Kadlec, P. & Kříž, J. A Dynamic Light Scattering Study of Fast Relaxations in Polymer Solutions. (2007). doi:10.1021/ma0620518
51. Štěpánek, P. & Johnsen, R. M. Dynamic Light Scattering from Polymer Solutions: The Subtraction Technique. *Collect. Czechoslov. Chem. Commun.* **60**, 1941–1949 (1995).
52. McNeil-Watson, F. Electrophoretic Light Scattering. in *Encyclopedia of Biophysics* 648–654 (Springer Berlin Heidelberg, 2013). doi:10.1007/978-3-642-16712-6_288
53. Banerjee, B., Misra, G. & Ashraf, M. T. Circular dichroism. in *Data Processing Handbook for Complex Biological Data Sources* 21–30 (Elsevier, 2019). doi:10.1016/B978-0-12-816548-5.00002-2
54. Seo, J. *et al.* An infrared spectroscopy approach to follow β-sheet formation in peptide amyloid assemblies. *Nat. Chem.* **9**, 39–44 (2017).
55. Bouchard, M., Zurdo, J., Nettleton, E. J., Dobson, C. M. & Robinson, C. V. Formation of insulin amyloid fibrils followed by FTIR simultaneously with CD and electron microscopy. *Protein Sci.* **9**, 1960–1967 (2000).
56. Reimer, L. *Transmission Electron Microscopy*. *Kobunshi* **36**, (Springer Berlin Heidelberg, 1984).
57. Fultz, B. & Howe, J. *Transmission Electron Microscopy and Diffractometry of Materials*. (Springer Berlin Heidelberg, 2013). doi:10.1007/978-3-642-29761-8
58. Ford, B. J., Bradbury, S. & Others. Transmission Electron Microscope. *Encyclopædia Britannica* (2019). Available at: https://www.britannica.com/technology/transmission-electron-microscope. (Accessed: 27th September 2020)
59. Gras, S. L., Waddington, L. J. & Goldie, K. N. Transmission electron microscopy of amyloid fibrils. *Methods Mol. Biol.* **752**, 197–214 (2011).
60. Ban, T., Hamada, D., Hasegawall, K., Naiki, H. & Goto, Y. Direct observation of amyloid fibril growth monitored by thioflavin T fluorescence. *J. Biol. Chem.* **278**,

16462–16465 (2003).
61. Xue, C., Lin, T. Y., Chang, D. & Guo, Z. Thioflavin T as an amyloid dye: fibril quantification, optimal concentration and effect on aggregation. *R. Soc. Open Sci.* **4**, 160696 (2017).
62. Khurana, R. *et al.* Mechanism of thioflavin T binding to amyloid fibrils. *J. Struct. Biol.* **151**, 229–238 (2005).
63. Srivastava, A. *et al.* Identifying the Bond Responsible for the Fluorescence Modulation in an Amyloid Fibril Sensor. *Chem. - A Eur. J.* **16**, 9257–9263 (2010).
64. Mishra, R., Sjölander, D. & Hammarström, P. Spectroscopic characterization of diverse amyloid fibrils in vitro by the fluorescent dye Nile red. *Mol. Biosyst.* **7**, 1232 (2011).
65. Doyle, M. L. Characterization of binding interactions by isothermal titration calorimetry. *Curr. Opin. Biotechnol.* **8**, 31–35 (1997).
66. Leavitt, S. & Freire, E. Direct measurement of protein binding energetics by isothermal titration calorimetry. *Current Opinion in Structural Biology* **11**, 560–566 (2001).
67. Pierce, M. M., Raman, C. S. & Nall, B. T. *Isothermal Titration Calorimetry of Protein-Protein Interactions*. *METHODS* **19**, (1999).
68. Cao, A., Hu, D. & Lai, L. Formation of amyloid fibrils from fully reduced hen egg white lysozyme. *Protein Sci.* **13**, 319–24 (2004).
69. Tokunaga, Y., Matsumoto, M. & Sugimoto, Y. Amyloid fibril formation from a 9 amino acid peptide, 55th-63rd residues of human lysozyme. *Int. J. Biol. Macromol.* **80**, 208–216 (2015).
70. Swaminathan, R., Ravi, V. K., Kumar, S., Kumar, M. V. S. & Chandra, N. Lysozyme: A model protein for amyloid research. *Adv. Protein Chem. Struct. Biol.* **84**, 63–111 (2011).
71. C. Crdenas-Aguayo, M. del *et al.* Physiological Role of Amyloid Beta in Neural Cells: The Cellular Trophic Activity. in *Neurochemistry* (InTech, 2014). doi:10.5772/57398
72. Khan, Z. U., Martín-Montañez, E., Navarro-Lobato, I. & Muly, E. C. Memory deficits in aging and neurological diseases. in *Progress in Molecular Biology and Translational Science* **122**, 1–29 (Academic Press, 2014).
73. Chen, G. *et al.* Amyloid beta: structure, biology and structure-based therapeutic development. *Acta Pharmacol. Sin.* **38**, 1205–1235 (2017).
74. Murr, L. E. & Soto, K. F. A TEM study of soot, carbon nanotubes, and related fullerene nanopolyhedra in common fuel-gas combustion sources. *Mater. Charact.* **55**, 50–65 (2005).
75. Rambabu, G. & Bhat, S. D. Sulfonated fullerene in SPEEK matrix and its impact on the membrane electrolyte properties in direct methanol fuel cells. *Electrochim. Acta* **176**, 657–669 (2015).
76. Nair, V. S., Mukhopadhyay, R. D., Saeki, A., Seki, S. & Ajayaghosh, A. A -gel scaffold for assembling fullerene to photoconducting supramolecular rods. *Sci. Adv.* **2**, e1600142–e1600142 (2016).
77. Mishra, R., Sjölander, D. & Hammarström, P. Spectroscopic characterization of diverse amyloid fibrils in vitro by the fluorescent dye Nile red. *Mol. Biosyst.* **7**, 1232 (2011).
78. Uversky, V. N. & Lyubchenko, Y. *Bio-Nanoimaging : Protein Misfolding & Aggregation*. (Elsevier Inc., 2013).

79. Ghule, A. V. *et al.* Carbon nanotubes prevent 2,2,2 trifluoroethanol induced aggregation of protein. *Carbon* **45**, 1586–1589 (2007).
80. Fu, Z., Luo, Y., Derreumaux, P. & Wei, G. Induced β-barrel formation of the Alzheimer's Aβ25-35 oligomers on carbon nanotube surfaces: Implication for amyloid fibril inhibition. *Biophys. J.* **97**, 1795–1803 (2009).
81. Li, H., Luo, Y., Derreumaux, P. & Wei, G. Carbon nanotube inhibits the formation of β-sheet-rich oligomers of the Alzheimer's amyloid-β(16-22) peptide. *Biophys. J.* **101**, 2267–2276 (2011).
82. McLaurin, J., Franklin, T., Zhang, X., Deng, J. & Fraser, P. E. Interactions of Alzheimer amyloid-β peptides with glycosaminoglycans. *Eur. J. Biochem.* **266**, 1101–1110 (1999).
83. Cohlberg, J. A., Li, J., Uversky, V. N. & Fink, A. L. Heparin and other glycosaminoglycans stimulate the formation of amyloid fibrils from α-synuclein in vitro. *Biochemistry* **41**, 1502–1511 (2002).
84. Stewart, K. L. & Radford, S. E. Amyloid plaques beyond Aβ: a survey of the diverse modulators of amyloid aggregation. *Biophys. Rev.* **9**, 405–419 (2017).
85. Liu, H. *et al.* Positively Charged Chitosan and N -Trimethyl Chitosan Inhibit Aβ40 Fibrillogenesis. *Biomacromolecules* **16**, 2363–2373 (2015).
86. Wang, P. *et al.* A glucan isolated from flowers of Lonicera japonica Thunb. inhibits aggregation and neurotoxicity of Aβ42. *Carbohydr. Polym.* **110**, 142–147 (2014).
87. Engelking, L. R. Glycogen. in *Textbook of Veterinary Physiological Chemistry* 147–152 (Elsevier, 2015). doi:10.1016/B978-0-12-391909-0.50023-2
88. Cole, L. & Kramer, P. R. Sugars, Fatty Acids, and Energy Biochemistry. in *Human Physiology, Biochemistry and Basic Medicine* 17–30 (Elsevier, 2016). doi:10.1016/b978-0-12-803699-0.00019-0
89. Brown, A., Baltan, S. & Ransom, B. R. Glycogen Metabolism in CNS White Matter. in *Encyclopedia of Neuroscience* 929–934 (Elsevier, 2009). doi:10.1016/B978-008045046-9.01732-0
90. Yasar Yildiz, S. & Toksoy Oner, E. Mannan as a Promising Bioactive Material for Drug Nanocarrier Systems. in *Application of Nanotechnology in Drug Delivery* **i**, 13 (InTech, 2014).
91. Moreira, L. R. S. & Filho, E. X. F. An overview of mannan structure and mannan-degrading enzyme systems. *Appl. Microbiol. Biotechnol.* **79**, 165–178 (2008).
92. Gilchrist, K. B., Garcia, M. C., Sobonya, R., Lipke, P. N. & Klotz, S. A. New Features of Invasive Candidiasis in Humans: Amyloid Formation by Fungi and Deposition of Serum Amyloid P Component by the Host. *J. Infect. Dis.* **206**, 1473–1478 (2012).
93. Pearsall, N. N. & Lagunoff, D. Immunological Responses to Candida albicans II. Amyloidosis in Mice Induced by Candidiasis. *Infect. Immun.* **10**, 1397–1400 (1974).
94. Marshall, K. E. *et al.* Hydrophobic, Aromatic, and Electrostatic Interactions Play a Central Role in Amyloid Fibril Formation and Stability. *Biochemistry* **50**, 2061–2071 (2011).
95. Podzimek, S. *Light Scattering, Size Exclusion Chromatography and Asymmetric Flow Field Flow Fractionation: Powerful Tools for the Characterization of Polymers, Proteins and Nanoparticles*. *Light Scattering, Size Exclusion Chromatography and Asymmetric Flow Field Flow Fractionation: Powerful Tools for the Characterization of Polymers, Proteins and Nanoparticles* (John Wiley & Sons, Inc., 2011). doi:10.1002/9780470877975

96. Nemzer, L. R., Flanders, B. N., Schmit, J. D., Chakrabarti, A. & Sorensen, C. M. Ethanol shock and lysozyme aggregation. *Soft Matter* **9**, 2187–2196 (2013).
97. Mambule, C. *et al.* Enhancement of AA-amyloid formation in mice by transthyretin amyloid fragments and polyethylene glycol. *Biochim. Biophys. Acta - Gen. Subj.* **1474**, 331–336 (2000).
98. Milowska, K. *et al.* Carbosilane dendrimers inhibit α-synuclein fibrillation and prevent cells from rotenone-induced damage. *Int. J. Pharm.* **484**, 268–275 (2015).
99. Cannon, J. R. *et al.* A highly reproducible rotenone model of Parkinson's disease. *Neurobiol. Dis.* **34**, 279–290 (2009).

7. Attached publications

Publications declaration

In all the publications included in the thesis, Monika Holubová

- synthesized CDs
- designed two model systems for testing amyloidogenicity
- performed all the testing of amyloidogenicity (ThT or NR fluorescence, data processing and fitting)
- performed DLS measuring and data processing
- as the first author, wrote most of the text in the all publications

The synthesis of GG modifications, more complex characterizations of species and ITC were performed in cooperation with colleagues (co-authors of publications) from the Institute of Macromolecular Chemistry CAS.